


PHOTOACOUSTIC SENSING OF BIO-ELECTRICAL ACTIVITY

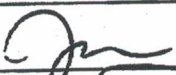
by

Nashaat S. Rasheed
A Dissertation
Submitted to the
Graduate Faculty
of
George Mason University
in Partial Fulfillment of
The Requirements for the Degree
of
Doctor of Philosophy
Bioengineering

Committee:

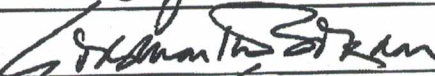

NALU Peixoto.

Dr. Parag V. Chitnis, Dissertation Director



Siddhartha Sikdar

Dr. Nathalia Peixoto, Committee Member

Dr. John R. Cressman, Committee Member

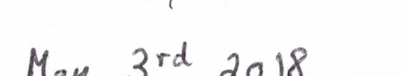

Patrick Vora

Dr. Siddhartha Sikdar, Committee Member


Michael Buschmann

Dr. Patrick Vora, Committee Member

Dr. Michael Buschmann, Department Chair


Kenneth S. Ball

Dr. Kenneth S. Ball, Dean, Volgenau School of Engineering

Date: May 3rd 2018

Spring Semester 2018
George Mason University
Fairfax, VA

Photoacoustic Sensing of Bio-electrical Activity

A Dissertation submitted in partial fulfillment of the requirements for the degree of
Doctor of Philosophy at George Mason University

By

Nashaat S. Rasheed
Master of Engineering
Cornell University, 2014
Master of Engineering
Huazhong University of Science and Technology, 2012
Bachelor of Science
American University of Science and Technology, 2007

Director: Dr. Parag V. Chitnis , Assistant Professor
Bioengineering Department

Spring Semester 2018
George Mason University
Fairfax, VA

Copyright: 2018 Nashaat S. Rasheed
All Rights Reserved

DEDICATION

I dedicate this dissertation to my wife Deema and my son Aiden, who supported me throughout this journey.

I also dedicate this dissertation to my brother, Shadi Rasheed, who believed in education and believed in me.

ACKNOWLEDGEMENTS

I would like to express my special thanks to my advisor Dr. Parag V. Chitnis for believing in me and for providing me the opportunity to be part of his research group. Your advice and continued support throughout my Ph.D. studies have been invaluable. I would also like to thank my committee members, Dr. Peixoto, Dr. Cressmann, Dr. Sikdar and Dr. Vora, for their continued support, help and inputs on improving my research skills. Thanks to Claudia Borke and Terry McGowan for all their support and help during these past years. Thanks to the Biomedical Imaging Laboratory (BMIL) family, the Bioengineering Department, and Krasnow Institute for Advanced Study. Without the Presidential Scholarship, Summer Research Fellowships, and Dissertation Completion Grant, the completion of this dissertation would have been very challenging.

Thanks to Dr. Nadine Kabani and Justin King for providing the PC12 cell culture. Thanks to Mara and Dr. Cressman for their collaboration and work especially with the cell patch clamp. Thanks to all my colleagues and friends who supported me: Monica, Shervin, Nima Ravi, and Linda.

A special Thank You goes to my family. Words cannot express how grateful I am to my lovely wife Deema and our son Aiden. Without your continued support and patience, I would not have made it this far. My mother Nada, my father Shawki, my brothers Shadi, Nizar, Sari, Makram, and Douraid.

TABLE OF CONTENTS

	Page
List of Tables	viii
List of Figures	ix
Abstract	xi
Chapter One: Introduction and background.....	1
1.1. <i>In vitro</i> recordings of electrical activity	3
1.1.1. Microelectrode arrays (MEAs)	3
1.1.2. Patch-clamp techniques	6
1.2. <i>In vivo</i> recordings of electrical activity	7
1.2.1. Utah arrays	8
1.2.2. Floating microelectrode arrays (FMA)	9
1.3. Optical imaging of brain activity	10
1.3.1. Imaging brain activity with CaSDs and GECIs	12
1.3.2. Imaging electrical activity with VSDs, GEVIs and GEVS-FPs	14
1.3.3. Imaging voltage with inorganic nanostructures	17
1.3.4. Optical energy penetration in tissue.....	19
1.4. Photoacoustic imaging of brain activity	21
1.4.1. Photoacoustic microscopy of vascular hemodynamics.....	23
1.4.2. Photoacoustic microscopy versus photoacoustic computed tomography ...	24
1.4.3. PA measurements with calcium-sensitive dyes (CaSDs)	27
1.4.4. PA measurements with voltage-sensitive probes (VSDs)	29
Chapter Two: Materials and methods	33
2.1. PC12 cell culture	33
2.2. Methods to induce a change in membrane-potential.....	35
2.2.1. Potassium chloride (KCl).....	35
2.2.2. Tetraphenylborate (TPB)	35
2.3. Voltage-sensitive dyes and probes	36
2.3.1. RH795 dye preparation and cell-labeling	36
2.3.2. RH155 dye preparation and cell-labeling	37
2.3.3. Cellular labeling with QD voltage-sensing probes	38

2.4.	The optical-absorption characterization setup.....	39
2.5.	The photoacoustic signal measurement setup	40
2.6.	Theoretical model.....	41
2.7.	Patch-clamp recording setup	45
Chapter Three: Photoacoustic sensing of bio-electrical activity using voltage-sensitive dyes		47
3.1.	Optical-absorption characterization of VSD-labeled cells.....	48
3.2.	Photoacoustic signal sensing of RH155-labeled cells.....	54
3.3.	Electrophysiological recordings and theoretical model	60
3.4.	Discussion	61
3.5.	Conclusion.....	63
Chapter Four: Quantum-dot-based voltage reporters for dual-modality sensing of bioelectric activity.....		64
4.1.	The QD-peptide-C ₆₀ construct	66
4.2.	QD-PA sensing of cell depolarization.....	68
4.3.	Calibration of QD-PL and QD-PA response versus voltage.....	74
4.4.	Discussion	76
4.5.	Conclusion.....	78
Chapter Five: Summary and future direction.....		80
References.....		85

LIST OF TABLES

Table	Page
Table 1 Parameters in the model and experimental PA measurements	43

LIST OF FIGURES

Figure	Page
Figure 1.1 A single-well MEA chip.....	5
Figure 1.2 Schematic of the different modes of the patch-clamp techniques.....	7
Figure 1.3 Utah electrodes	9
Figure 1.4 Floating microelectrode arrays (FMA).....	10
Figure 1.5 Schematic diagram depicting fluorescence	11
Figure 1.6 Schematic of E-PEBBLEs	17
Figure 1.7 Tissue Transparency window.....	20
Figure 1.8 Illustration of photoacoustic (PA) signal generation in tissue.....	23
Figure 1.9 Schematics of OR-PAM and AR-PAM.....	25
Figure 1.10 Illustrations of cylindrical-view PACT; planar-view PACT and spherical-view PACT.....	26
Figure 1.11 Schematics of linear-view PACT and circular-view PACT.....	27
Figure 1.12 PA neuroimaging using calcium-sensitive probes	28
Figure 1.13 PA neuroimaging using voltage-sensitive probes	30
Figure 2.1 Staining of live intact rat PC12 pheochromocytoma cells with VSD	37
Figure 2.2 An image of cells labeled with the QD construct.....	38
Figure 2.3 Schematic of the optical-absorption characterization setup	39
Figure 2.4 Schematic of the PA measurement setup	41
Figure 2.5 KCl concentration conversion into membrane potential	45
Figure 2.6 Schematic of the patch-clamp recording setup.....	46
Figure 3.1 Optical absorption spectra of RH795 dye	48
Figure 3.2 Absorption spectra of RH795-labeled cells.....	49
Figure 3.3 Spectral shift of RH795-cells relative to 532-nm as a function of TPB.....	50
Figure 3.4 Absorption spectra of RH155-cells as a function of KCl concentrations	51
Figure 3.5 Fractional changes in optical-absorption (experimental versus modeled data) of RH155-cells at 690 nm as a function of time after administering KCl	52
Figure 3.6 Fractional change in absorption of the RH155-cells as a function of time as KCl and sucrose were administered.....	53
Figure 3.7 PA RF-line of RH795-cells and control cells.....	54
Figure 3.8 PA signals of RH155-cells and control cells.....	56
Figure 3.9 Fractional change in PA signal of RH155-labeled cells as a function of time with the administration of 2.5 mM KCl	57
Figure 3.10 Fractional changes in the experimental and modeled PA signal of RH155-cell as a function of KCl-induced depolarization	58
Figure 3.11 Fractional change in the PA signal of RH155-cells as a function of time with administering KCl and sucrose	59
Figure 3.12 Time evolution of cell-membrane potential of a patched PC12 cell and calculated cell-patch model.....	60

Figure 4.1 QD-peptide-C ₆₀ bioconjugates.....	67
Figure 4.2 Absorption and PL spectrum of the QD-peptide-C ₆₀ bioconjugate.....	68
Figure 4.3 PA signal of the QD-labeled cells	69
Figure 4.4 Fractional change in PA signal of the QD-labeled cells as a function of time with a 40 mV increase in cell membrane potential.....	70
Figure 4.5 Fractional change in the PA signal of QD-labeled cells as a function of cell potential.....	71
Figure 4.6 Fractional change in PA signal of QD-labeled cells as a function of time while administering KCl and sucrose	72
Figure 4.7 Fractional change in QD-PA signal as a function of QD concentration.....	73
Figure 4.8 Fractional change in QD-PL as a function of cell membrane potential	74
Figure 4.9 Fractional changes in PA-signal (experimental versus modeled data) of QD-labeled PC12 cells as a function of membrane potential change.....	75

ABSTRACT

PHOTOACOUSTIC SENSING OF BIO-ELECTRICAL ACTIVITY

Nashaat S. Rasheed, Ph.D.

George Mason University, 2018

Dissertation Director: Dr. Parag V. Chitnis

Optical-fluorescence imaging provides molecular specificity and spatio-temporal resolution necessary for noninvasive imaging of cellular interactions and bio-electrical activity. However, these techniques suffer from limited imaging depth constrained by optical absorption and scattering in tissue. This research investigates the feasibility of photoacoustic (PA) sensing of biopotentials, which relies on absorption of light by voltage-sensitive probes and subsequent generation/detection of ultrasound. PA-based voltage sensing could noninvasively provide voltage maps with spatial and temporal resolutions that are adequate for monitoring changes in neuronal cell-membrane potential in intact functional circuits. We have demonstrated the detectability and sensing of bio-electrical activity using PA-based voltage sensing. We have achieved this in two ways: (a) by characterizing the optical-absorption properties of voltage-sensitive dyes as a function of membrane potential change using a custom absorption spectrophotometer, and (b) by using *in vitro* experiments involving cell cultures to demonstrate that the photoacoustic signal from cells labelled with voltage-reporting probes track the change in cell potential. Pheochromocytoma (PC12) cells were tagged with voltage-sensitive probes such as the

commercially available voltage-sensitive absorption dye RH155 and a novel voltage-reporting nano-construct consisting of a CdSe-CdS/ZnS core-shell quantum dot (QD) conjugated to a peptide-fullerene bioconjugate. Cells were depolarized by administering potassium chloride (KCl), which was verified using whole-cell patch-clamp. A spectrophotometer was used to characterize the corresponding change in optical absorption. PA-signal amplitude exhibited a monotonic change with increasing cell-membrane potential and the dynamics of the PA-signal change was consistent with the theoretically modelled change in membrane potential. In summary, we have shown that PA-based voltage sensing can provide signal-to-noise-ratio and temporal response that are comparable to fluorescence sensing. When biopotentials were chemically altered in cell cultures, the photoacoustically measured voltage exhibited the same temporal dynamics as those observed by fluorescence. The methodologies developed in this research effort can potentially alleviate challenges encountered in current fluorescence-based techniques, and facilitate the study of neurological activity in healthy, diseased, and injured brain in intact biological models.

CHAPTER ONE: INTRODUCTION AND BACKGROUND

The study of the human brain and its function is one of the most fascinating and complex fields of science. The multidisciplinary effort of science and engineering has assisted us in understanding the basic neuronal principles of perception and motion. Employed methods such as patch-clamp technique [1], [2], microelectrode arrays (MEAs) [3]–[7], and optical-fluorescence imaging techniques [8]–[11] are well-adapted and the development of new methods and their application have gained new insights. The most widely used optical-fluorescence imaging methods of neuro-electrical activity involve labeling with voltage-sensitive dyes (VSDs) [12]. These fast voltage-sensitive dyes (VSDs) are cell-membrane-bound, opto-chemical probes that change their fluorescence or absorbance in response to membrane potential changes [12]–[15].

Deep brain stimulation is an effective method used to alleviate the symptoms of patients suffering from neurological disorders such as Parkinson's disease, obsessive compulsive disorder (OCD), depression, mental illness, and/or epilepsy by applying pulses of voltage or current to particular deep regions in the brain [16]. To measure the action potential and record the neural activity, different methods have been applied including: (a) extracellular recording, (b) intracellular recording, (c) optical imaging, and (d) techniques designed to record signals of extensive neural populations (electroencephalography,

magnetoencephalography, functional magnetic resonance imaging (fMRI), and electrocardiography) [16].

Intracellular and extracellular recording are two prime electrophysiology methods that have been employed for measuring action potential and realization of neural information processing in neural circuits. Intracellular recording is more suitable for sensitive recording, but it needs splitting a part of the plasma membrane to approach the cell cytoplasm directly. Therefore, intracellular recording is a highly invasive method and is difficult to perform causing significant limitations for long-term or large-scale recording. Extracellular recording is a non-invasive method and supports long-term recording; however, the weakness in signal strength and poor quality of the recorded signals are significant limitations of this method. For recording of action potential, microelectrodes should be close to neurological target cells. The signal-to-noise ratio (SNR) has an inverse relationship with the electrode impedance, as lower impedance is equivalent to having higher SNR. Furthermore, amalgamation of high impedance of the electrode and the distribution of the capacitance between the recording amplifier and the electrode leads to a reduction of high frequency response of the electrode [16].

The use of electrical stimulation of neural tissue goes back to the time of the invention of electricity. Electrical shock with 400 V from catfish was used for pain relief and as a treatment of several diseases by Ancient Egyptians. Fuzzy concept was introduced in 1791 by Luigi Galvani illustrating the electricity in an animal's body after electrically stimulating frog legs. In the year 1939, a major development in the design of neural interface occurred when Hodgkin and Huxley studied the electrical signals recorded from

single neural fiber by reduction of neural interface size. In 1960, an important attempt in use of the neural interface system was done by Evarts when electrophysiological experiments were conducted on the primary motor cortex of springy monkeys. Evarts pointed out that the firing rate of solitary neurons highly corresponded with the force created by the joints of the moving arm. Another significant transitional step in neural interface design and application took place in 1985, when micro-wire array electrodes came into force when dealing with a large number of patients [16].

1.1. *In vitro* recordings of electrical activity

The *in vitro* electrophysiological techniques are useful methods and amenable to different tissues and cell configurations. These techniques are capable of assessing changes in ion channel activity from the level of a single cell to a complex neuronal network [17]. Microelectrode arrays (MEAs) and patch-clamp techniques are considered the state-of-the-art techniques for *in vitro* recording of electrical activity.

1.1.1. Microelectrode arrays (MEAs)

Neural interfaces need to be implanted deeply in the brain to record the action potentials of neurons; therefore, the implantation process will be accompanied by significant clinical risks represented by tissue damage and infection of target sites. For less tissue damage and accurate long-term recording, implanted interfaces with the smallest cross section and the largest number of electrode sites are the ideal interfaces. Microelectrodes are used to stimulate neurons as well as signal recording [16]. MEAs [18]–[21] are the most important component in the brain–machine interfaces as they act in a way

that facilitates direct contact between the neural tissue and the electrical sensor. To obtain harmonious signals recorded from small clusters of neurons with retention of micro-stimulation abilities, MEAs are fabricated in a way that enables them to provide a low impedance path for the charge movement represented by charge injection and charge transformation. For low impedance, MEAs were made of highly conductive materials and fabricated in specific geometries. To decrease the impedance of the microelectrode and improve the neural recording, porous structures such as carbon nanotubes, Pt-black and high-conductive polymers were employed to increase the effective surface area of the exposed part of the electrode [16], [18].

Neuroscientists have traditionally relied on measuring the membrane potential using electrodes because neurons communicate electrically. Microelectrode arrays (MEAs) have been commonly used to record extracellular potentials from *in vitro* neuronal circuits [4], [18], [22]. MEAs have been used since the early 1970s to measure field potentials from neuronal cell cultures and tissue slices. MEAs make it possible to study the neuronal network activity instead of single cells measured using patch clamp analysis [23]. Furthermore, MEAs serve as test-platforms for drug screening, cell-based biosensors, and toxicological studies [4], [18], [23]. The current MEAs typically consist of 30-160 electrodes with inter-electrode spacing of 100-500 μm . Several commercially available MEAs are fabricated by thin-film technology with platinum (Pt), gold (Au), indium tin-oxide (ITO), titanium nitride (TiN), and iridium oxide (IrOx) microelectrode embedded in an insulation layer of polyamide, Si_3N_4 , and EPON SU-8 [4]. The cells are directly cultured

on the arrays allowing long-term (up to several months) monitoring and stimulation of the network electrophysiological activity [4].

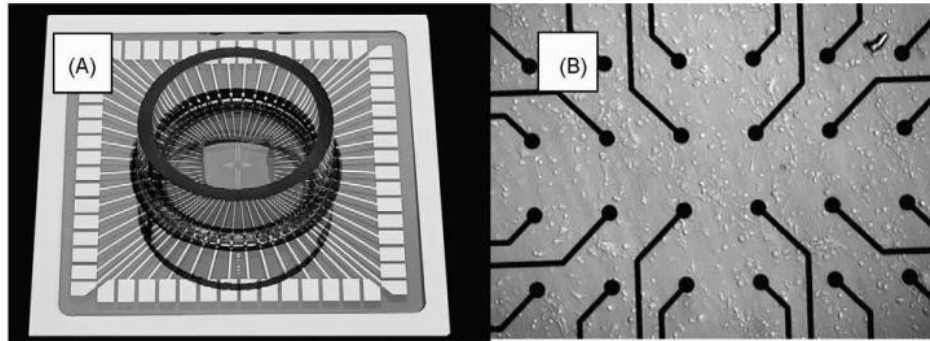


Figure 1.1: (A) A single-well MEA chip (the array contains 60 electrodes, including an internal ground electrode. Each electrode is 30 μm in diameter and the spacing between electrodes is 200 μm). (B) Photomicrograph of rat frontal cortex cells growing on a standard MEA [5].

MEAs have been applied to measure neuro-electrical activity *in vitro* and *in vivo*. The main advantage of MEAs is the capability to record and stimulate neurons at multiple sites simultaneously [24]. However, MEAs detect signals from all possible sources around every sensor [24]. Electrical recordings have significant limitations in studies of thousands of cells that form neuronal circuits, where only highly invasive electrode arrays can be used to record electrical activity [11]. Optical techniques seem to be an attractive solution for detecting membrane potential changes, since they are relatively noninvasive and can work at low and high magnification.

1.1.2. Patch-clamp techniques

Developed in the late 1970s, patch clamping has enabled the measurement of ionic currents on isolated cardiomyocytes down to the single-channels level [1], [25]. Patch clamping technique is the most precise for single-cell assay. The principle of patch-clamp technique has been described by Ogden and Stanfield in 1994 [25] and by Karmazina and Lacinova in 2010 [26]. The measurements can be done either on the whole-cell or single-channel level (cell-attached, inside-out or outside-out). The whole-cell patch-clamp technique is achieved by rupturing the patch of the isolated membrane by a patch pipette that brings the cell interior into contact with the pipette interior [25]. The whole-cell recording is the most widely used technique and can operate in two recording modes depending on the amplifier's configuration [26]. In the current-clamp mode, the input is the current that is injected into the examined cell and the recordings are either spontaneous action potentials (APs) in spontaneously active cells or APs in spontaneously inactive cells simulated by short current pulses. In the voltage-clamp mode, the ionic membrane current can be measured and the controlled input is the membrane voltage delivered to the cell [1], [26].

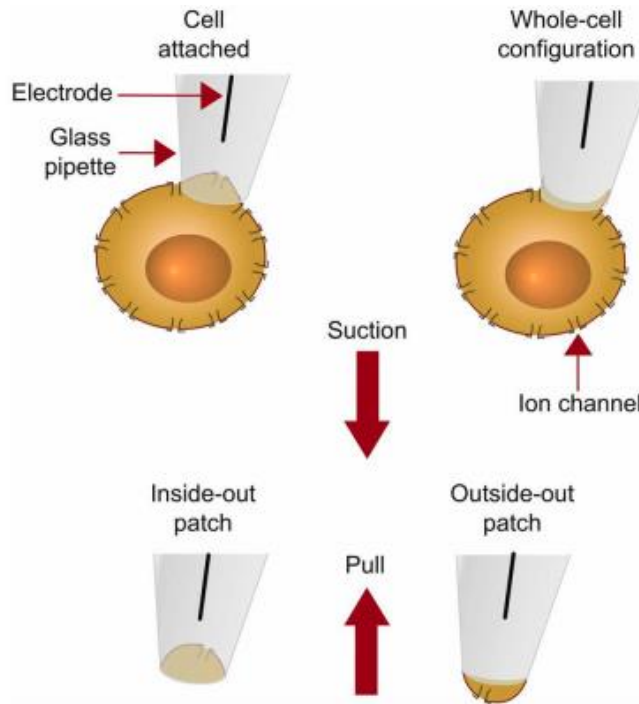


Figure 1.2: Schematic of the different modes of the patch-clamp techniques (cell-attached, whole-cell, inside-out patch, and outside-out patch mode) [27].

The most prominent advantage of patch clamping is its ability to report on a single-cell's electrical properties with high precision. However, patch clamp technique does not allow multiple recordings from *ex vivo* bulk tissue, thus suitable for culture preparations. Furthermore, it is an invasive method that leads to cell death within hours after patching the membrane due to its irreversible damage.

1.2. *In vivo* recordings of electrical activity

The state-of-the-art *in vivo* electrophysiological recordings of electrical activity are mostly performed with micro-fabricated arrays of metal electrodes such as Utah arrays,

silicon probes and tetrodes [28]. These metal electrodes capture the local field potentials (LFPs) generated by the spatiotemporal summation of current sources in the brain. In this section, two of the *in vivo* recordings of brain activity will be discussed: Utah arrays and floating microelectrode arrays (FMA).

1.2.1. Utah arrays

There is a big variety of implantable MEA architectures [19], [29], [30] with several designs: Utah electrode array [31] which consists of fabricated sharp tapered electrodes on a flat surface that are engineered for *in vivo* studies to be inserted from above in tissues (Figure 1.3 shows flat and inclined Utah electrodes); flattened shank electrodes with 10-30 μm metal pads on both sides and placed 10-100 μm apart [32], [33]; or electrodes that are uniformly distributed on a flat substrate for planar recordings [34], [35]. These MEA architectures provide a versatile tool for sensing local field potentials and acute spikes at millisecond time scale. The main advantage of these instruments is its ability to sense electrical signals of tens of microvolts at $\sim 100 \mu\text{m}$ distance away from the sources which makes MEAs one of the most quantitatively robust extracellular voltage measurement methods [36]. However, the non-specificity of MEAs hinders them to control precise neuronal dynamics [29].

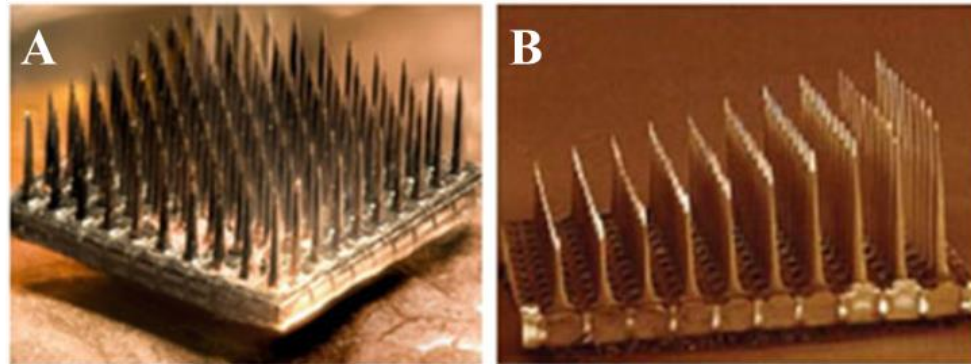


Figure 1.3: Utah electrodes. Flat array (A) and incline array (B) [16].

1.2.2. Floating microelectrode arrays (FMA)

The human brain has a highly convoluted structure and the need to access various surfaces and deep areas is essential. Researchers have developed arrays with electrodes of arbitrary lengths for deep neuronal recordings [37]. These microelectrode arrays are not anchored to the skull and thus “floats” on the brain [37], [38]. Floating microelectrode arrays (FMA) is a sophisticated neural interface that is suited for chronic recording and stimulation in small and large animal cortex. FMA’s small size, flexibility and low profile made it ideal for the implementation of large number of arrays simultaneously in the same animal that allows targeting multiple cortical locations at the same time [37], [38]. The length and impedance of individual electrodes within the same array are customized, thus allowing multiple cortical layers’ and deep structures’ recording and collecting LFP from the same cortical region [37]. Figure 1.4 shows short and long electrodes of different FMAs and a scanning electron microscope (SEM) image of an individual FMA electrode.

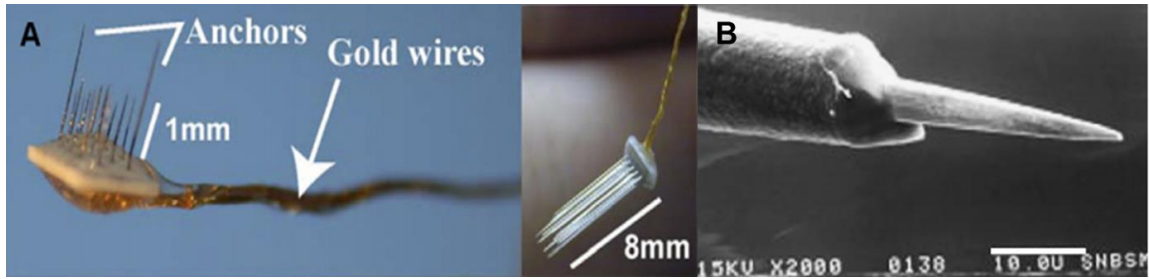


Figure 1.4: (A) FMAs with short and long electrodes: the two long anchors on the short arrays (1.4A, left image) are there to ensure that the arrays stay in the brain. (B) An SEM image of an electrode used in the FMA [37].

In comparison to the traditional electrophysiological techniques stated above, optical-based techniques have the ability to noninvasively measure action potentials (AP), customize field-of-view and resolution to probe a single neuron or a large neuronal network.

1.3. Optical imaging of brain activity

Optical imaging is one of the most well-developed methods to observe the smallest biological structures at the highest achievable resolution. Optical techniques overcome several of the shortcomings of electrophysiological approaches. Since the light can be delivered and sensed noninvasively on temporal and spatial scales that can span several orders of magnitude, optical-fluorescence imaging can offer many unique features for measuring neuro-electrical activity [39]. Figure 1.5 below illustrates the basic physics underlying the fluorescence process which is better explained by the Jablonski diagram [40]. The Jablonski diagram is an energy diagram, arranged with energy on a vertical axis and the rest of the diagram is arranged into columns. Within each column, horizontal lines

represent eigenstates for a particular molecule [40]. For instance, one pathway for molecules to deal with received energy is to release a photon, this is called fluorescence. Fluorescence is a slow process on the order of 10^{-9} to 10^{-7} seconds and thus it is not likely for an electron to dissipate energy [40]. Fluorescence is observed between the first excited electron state and the ground state. Since the emitted photon has less energy than the absorbed photon it is at a longer wavelength. This explains the process of fluorescence that converts light of one wavelength (shorter) to another wavelength (longer) [40].

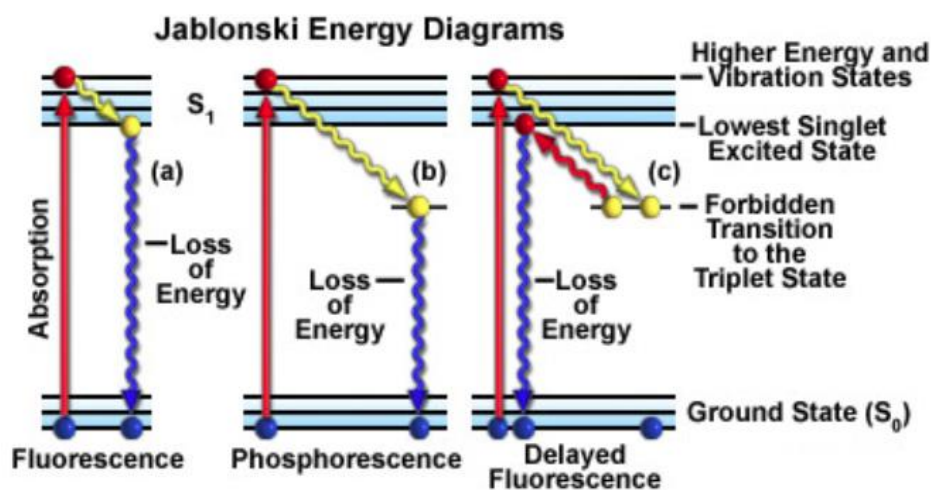


Figure 1.5: Schematic diagram depicting fluorescence (A), phosphorescence (B) and delayed fluorescence mechanism (C) [40].

Many fluorescent probes have been developed using variants of *Aequorea Victoria* green fluorescent protein (GFP) [41]. These fluorescent probes have enabled fluorescence imaging of cell activity and advanced our understanding of the spatiotemporal regulation of biological functions inside the neurons and the brain [41]. Theoretically speaking, the

selective introduction of genetically encoded fluorescent probes into neurons should increase the sensitivity of neuronal optical imaging. Scattering prevents the penetration of visible light into the brain tissue and near-infrared (NIR) light at 650-950 nm wavelengths can travel further than visible light since NIR light is less absorbed by hemoglobin [41]. NIR fluorescent proteins have not yet been achieved; therefore, organic dyes such as diaminocyanines (DACs) are the best probes for NIR fluorescence imaging [41].

1.3.1. Imaging brain activity with CaSDs and GECIs

Calcium is a universal second messenger that regulates cell signaling pathways involved in neurotransmitter release, cellular metabolism, muscular contraction, apoptosis, etc. [42]. Abnormalities in the regulation of calcium signaling have pathological consequences that are relevant to common ailments such as Alzheimer's, cardiovascular disorders and cancer [42]. Fluorescent calcium indicators or calcium-sensitive dyes (CaSDs) were first introduced by Tsien et al. in 1982 [43]. CaSDs are molecules that respond to the binding of calcium by changing their fluorescent properties. These fluorescent CaSDs have been widely used to analyze cellular calcium responses and investigate calcium signaling within living cells [44]. Calcium imaging can probe cortical dynamics *in vivo* including neuronal activity and metabolic signaling. For example, wide-field single-photon calcium imaging has been used to measure population neuronal activity [45]. Furthermore, the calcium signal can be recorded simultaneously with intrinsic optical imaging, thus allowing measurements of cerebral blood volume (CBV) changes [45].

The development of CaSDs for noninvasive cell loading allowed much broader use of calcium imaging. The next leap in calcium imaging technology was the introduction of

genetically encoded calcium ion indicators (GECIs) that have become widely useful tools for *in vitro* and *in vivo* calcium imaging [46], [47]. GECIs can be divided into two categories based on the number of fluorescent proteins (FPs) present in the indicator. Some GECIs contain a single FP and they involve a change in fluorescence intensity upon calcium binding. Other GECIs contain two FPs and monitoring calcium dynamics using these particular GECIs takes advantage of the concept of fluorescence resonance energy transfer (FRET) technique [46]. During FRET, one of the FPs acts as a donor and transfers the absorbed energy to the second FP (acceptor) when it is excited. The efficiency of FRET is dependent on the distance between the donor and the acceptor moieties; therefore, it can be only used at distances ~ 10 nm. In this case, GECIs are designed in such a way that FRET efficiency increases after calcium binding either due to changing in their relative orientations or to approaching the two FP moieties each other [46].

Optical imaging with CaSDs and GECIs are powerful tools for measuring intracellular calcium concentration with good spatiotemporal resolution. The brightness of fluorescent calcium indicators gives signals with good signal-to-noise-ratio (SNR). However, there are various issues (such as photobleaching and photo-damage) to ensure optimal quantitative data output and minimal cell invasiveness [44]. CaSDs are unable to cross the lipid membrane easily due to their charged nature [48]. CaSDs label the cytoplasm and are thus considered as an indirect measurement of brain activity. On the other hand, VSDs stain the plasma membrane and therefore track the changes in the membrane potential directly. VSDs incorporated into the cell membrane are particularly attractive

voltage-sensitive probes due to their ability to measure membrane potentials in specific type of cells with high sensitivity and fast temporal response.

1.3.2. Imaging electrical activity with VSDs, GEVIs and GEVS-FPs

Voltage-sensitive dye (VSD) imaging is a powerful technique that enables visualization of neural circuit functions with reasonable spatial and temporal resolution [14], [49]. The optical-signal intensity and the transmembrane voltage changes are linearly correlated; thus optics can be used to measure neuro-electrical activity without using traditional electrophysiological techniques [14]. VSD-based fluorescence imaging is a useful tool for imaging cellular electrical activity, but current techniques are limited to penetration depths of less than 1 mm [50]. VSDs are attractive probes due to their ability to measure membrane potentials in specific type of cells with high sensitivity and fast temporal response. To overcome some of the challenges in applying voltage sensors *in vivo* is to use different imaging modalities such as PA imaging which helps to deal with the scattering and photobleaching *in vivo* [50].

VSDs are being increasingly employed in neuroscience for the visualization of voltage transients in membrane potential [13]. It has been reported that the VSDs respond to changes in the membrane potential by electrochromic effect [11], [13], [51]–[54], reorientation/solvatochromic mechanisms [11], [14], [15], and/or electro-optical phenomena [11], [14]. The fast absorbance VSD RH155 has been applied in vertebrate slice [55], [56], invertebrate ganglia [57], and cell culture preparations [58], [59]. In addition, the fast response time of RH155 dye makes it advantageous in resolving individual action potentials [60].

Although VSDs monitor cell membrane potential changes in mammalian brain tissue with high temporal and spatial resolution, these dyes lack cell-label specificity [61]. Optogenetics techniques have helped overcome such limitations of VSDs and encouraged the design and development of voltage-sensitive probes based on fluorescent proteins (FPs) [61]. Akemann W. et al. developed a fluorescence resonance energy transfer (FRET)-based voltage-sensitive FPs named VSFP2s that have efficient targeting to the cell surface and are very responsive to cell membrane potential change in cultured cells. Monitoring electrical activity using fluorescent probes is a tradeoff between SNR and interference with the system's operation. For example, GE-Ca indicators affect the calcium dynamics by buffering calcium and very likely to interfere with cellular process by interacting with endogenous signaling pathways. In the contrary, VSDs have direct photobleaching and phototoxic effects [61].

VSDs monitor membrane-potential changes from single or multiple neurons in mammalian brain tissue with high spatiotemporal resolution; however, these probes are generally not suitable for labeling of specific cell populations [61]. Emerging optogenetics methods motivated the development of voltage-reporting probes based on fluorescent proteins [62]. Genetic engineering permits the precise control of the expression of such protein probes to selected cell population and therefore disables background noise and enables the assignment optical response signals to defined cellular sources [61]. Akemann W. et al. developed fluorescence resonance energy transfer (FRET)-based voltage-sensitive fluorescent proteins (VSFPs) with high responsiveness to membrane-potential signaling in cultured cells and with effective targeting to the cell surface [61]. On the other

hand, Gong Y. et al introduced FRET-opsin florescent voltage sensors to address the challenges of sensing voltage with bright and rapid optical sensors [9]. They imaged neural spiking and sub-threshold membrane voltage dynamics in cultured neurons and tissue slices using FRET-opsin sensors. These FRET-opsin sensors improve upon the spike detection reliability offered by the genetically encoded voltage sensor, ArcLight, while offering faster kinetics and higher brightness [9].

Some work also involved the encapsulation of voltage-sensitives probes in micelles [63]. Photonic explorer for biomedical use with biologically localized embedding (PEBBLE) technology has been used to measure calcium, potassium, oxygen, nitric oxide, etc. inside cultured cells [64]. The emergence of electro-PEBBLEs (E-PEBBLEs) permits the use of multiple sensor systems in living cells to simultaneously determine the chemical and physical properties of biological processes [63]. E-PEBBLEs are nanoparticles that measure electric fields with the aid of photons. The design, synthesis and application of these nanosized “photonic voltmeter” was first reported in 2007 by Tyner *et al.* in which they are not confined to the exploitation of the properties of lipid bilayers during changes in electric fields [63].

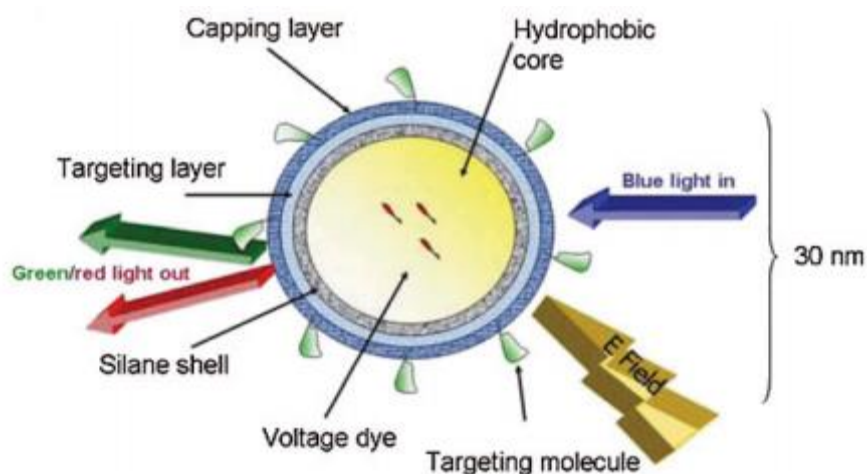


Figure 1.6: Schematic of E-PEBBLEs. The voltage-sensitive dye is encased in a saline-capped micelle. The uniform environment allows the nanoparticles to be externally calibrated before delivery to the cells [63].

1.3.3. Imaging voltage with inorganic nanostructures

1.3.3.1. Plasmonic nanostructures

Simple plasmonic metallic nanoparticles such as gold nanorods and nanoshells exhibit small ($\sim 5\text{-}10\text{ nm}$) localized surface plasmon resonance (LSPR) shifts upon voltage changes ($\sim 0.5\text{V}$) [65]–[67]. LSPR is a collective oscillations of electrons in metallic nanoparticles that have been used in various applications that relied on spectral shifts of the plasmon resonance due to the electrodynamic coupling among adjacent particles [65], [68]. Researchers applied an electrostatic field sensing technique for detecting activity in mammalian brain neural cells, by optically measuring the cellular potential induced shift in the surface plasmon resonance mode of an adjacent planar gold nanoparticle array [66]. Zhang *et al.* demonstrated real time detection of hippocampal neural spiking activity by the

LSPR shift in an embedded gold nanoparticle optical probe, opening up the possibility of extending the use of metallic nanoparticles for *in vivo* applications for all-optical recording [66]. Unlike metals, plasmon resonance frequencies of doped semiconductors can be modified by changing the composition of the material. Well-defined LSPR features have been observed in the infrared spectra of highly doped semiconductor nanocrystals such as tin-doped indium oxide (ITO) with lower concentration of free carriers with larger LSPR shifts compared to metallic nanostructures [69].

1.3.3.2. Semiconductor nanostructures

Optical methods, that are capable of reporting the electrophysiological dynamics of large-scale neural networks with millisecond temporal resolution, have been pursued. The existing voltage-sensitive fluorescent sensors (synthetic organic and genetically encoded voltage sensors) can detect action potentials in individual cultured neurons; however, limitations in their brightness and dynamic range have hindered monitoring of spiking activity across large population of individual neurons [70]. There are few reports on semiconductor nanoparticles such as quantum dots (QDs) that have been used to image electric fields. In 2008, Invitrogen scientific group reported the potential application of QDs as voltage-sensitive probes due to their physical size that is comparable to the cell membrane thickness and the potential tenability of their electronic properties to the external electromagnetic field [71]. Some work using semiconductor QD dye complexes exploiting FRET [72] or big micelles with enclosed QDs [63] opens the possibility of QD applications towards probing electrical activity.

In 2010, Bardi *et al.* developed and characterized amino functionalized CdSe/ZnS QD-doped silica nanoparticles with gene carrier and imaging capabilities [73]. They showed that the QD-doped silica NPs can be used in the brain and are internalized by primary cortical neural cells without inducing cell death *in vitro* and *in vivo* [73]. In 2013, Marshall and Schnitzer reported an inorganic class of fluorescent voltage sensors, a semiconductor ultra-bright multifunctional quantum dots (QDs) and other semiconductor nanocrystals, for sensing neural electrical dynamics [70]. These QDs offer cross sections for one-photon and two-photon absorption that are ~ 10 -100 times and 100-1000 times greater than those of VSDs, respectively [70].

1.3.4. Optical energy penetration in tissue

With medical advancements and applications of laser, understanding of the propagation of light and deposition of energy in biological tissue become crucial for effective diagnosis and therapy. Living tissues are a highly-complex, dynamic turbid medium, with optical properties of which are defined by varying rates of absorption, scattering, transmission and reflection [74]. In other words, the parameters used to characterize the optical properties of the tissue are: the absorption coefficient (μ_a in cm^{-1}), the scattering coefficient (μ_s in cm^{-1}), the transport coefficient ($\mu_t = \mu_a + \mu_s$), and the phase function $p(s, s')$ [75]. Imaging techniques such as optical-fluorescence imaging rely upon an understanding of these complex optical properties. Penetration of light in living tissue depends on various parameters including wavelength, intensity, power, tissue contact, compression, polarization and coherence [75].

As the wavelength increases, the scattering coefficient of tissue decreases monotonically, while the absorption coefficient varies over the visible spectrum due to the presence of chromophores. For instance, blood and water usually dominate the absorption spectrum; and fat and melanin must be considered in relation to the visible part of the spectrum. The domination of the blood optical absorption is due to oxygenated and deoxygenated hemoglobin. The oxy-hemoglobin absorption spectrum peaks between 400 nm and 600 nm and the deoxy-hemoglobin peaks between 400 nm and 850 nm (see Figure 1.7 below).

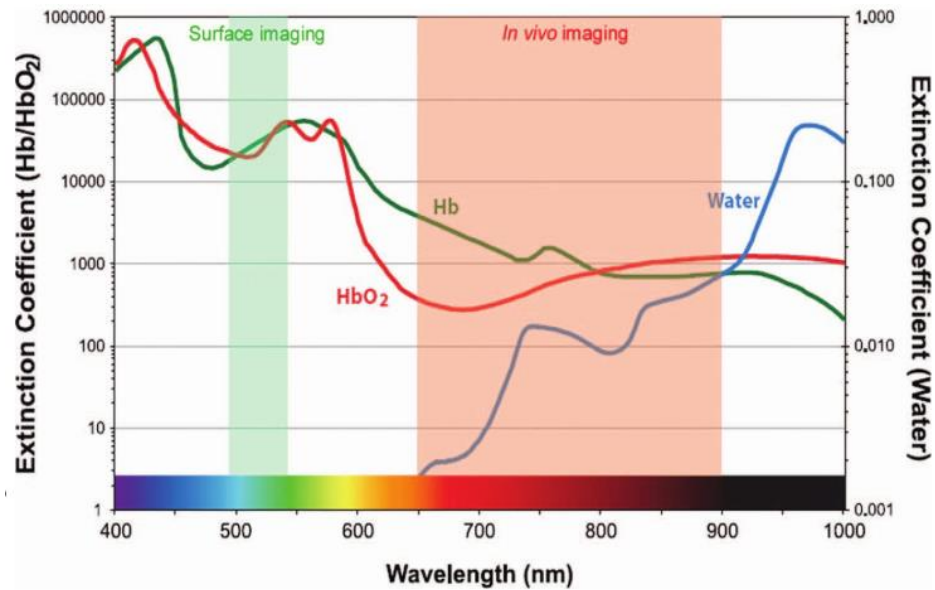


Figure 1.7: Tissue Transparency window [76].

Reported measurements via fluorescent probes are photon limited and scanning techniques such as two-photon microscopy and confocal microscopy collect light from a

single point in the tissue at a time [39]. The development of microscopy techniques with kHz bandwidth to capture action potentials (APs) has been needed. Optical fluorescence-based methods are considered attractive techniques due to their ability to image electrical activity noninvasively. However, they also have some limitations: (1) restricted imaging depth that is limited to ballistic-photon regime (under 0.5 mm) due to optical scattering in tissue; (2) photo-toxicity due to required high-intensity excitation to establish an adequate fluorescence signal; and (3) sub-optimal signal-to-noise ratio (SNR) due to low quantum yield.

Photoacoustic imaging (PAI) relies on the absorption of light by chromophores that leads to subsequent generation of ultrasound from within the tissue. Since the functional information is relayed to the sensor acoustically, PAI is less susceptible to optical-scattering in the tissue as optical fluorescence-based imaging. Therefore, PAI offers deeper imaging of chromophores and could be an attractive alternative to fluorescence-based imaging.

1.4. Photoacoustic imaging of brain activity

Photoacoustic (PA) imaging (PAI) is a noninvasive hybrid imaging modality that relies on the optical absorption by biological tissue molecules and ends with ultrasonic detection of acoustic waves which are generated through rapid thermos-elastic expansion. The PA signal is sensitive to the optical absorption contrast of biomolecules and the resulted acoustic waves are not as sensitive to scattering as light. Therefore, PAI combines the specificity of optics with the resolution and depth of ultrasound [77]–[82]. PAI, with its advantages over the optical-fluorescence, is considered an attractive alternative for

imaging the brain and neuro-electrical activity [77], [78], [83]. PAI provides noninvasive high-resolution (20-100 μm) images of the brain in a preclinical setting at $\sim 100 \mu\text{s}$ temporal resolution [78]. The PA image contrast is determined by the absorbed light properties by the tissue and the imaging frame rate is limited by the laser's pulse repetition rate (10 Hz to 5 kHz) and the speed of sound in tissue (1.5 mm/ μs). The design and development of optical contrast agents such as chemical dyes [84], fluorescence proteins [85], [86] and nanoparticles [87] allow PA molecular brain imaging [78].

In photoacoustic sensing (PAS), incident optical energy is converted into sound through localized heating and the mechanism in generating acoustic signal involves local absorption of optical energy, localized heating, and subsequent thermoelastic expansion. Photoacoustic (PA) signal sensing is based on absorption of light and the general photoacoustic equation as described by Rao et al. [88] is

$$p = \alpha \xi \Gamma m \mu F$$

Where p denotes the received photoacoustic signal; α is a spatially dependent factor; ξ is a coefficient that represents the attenuation and distortion of the PA signal; Γ is the Gruneisen parameter of the medium; m is the dye's molar concentration; μ is the optical absorption coefficient of RH-155, and F is the optical fluence. The plasma membrane potential does not change α , ξ , Γ , and F . Figure 1.8 below illustrates the generation of PA signal in tissue.

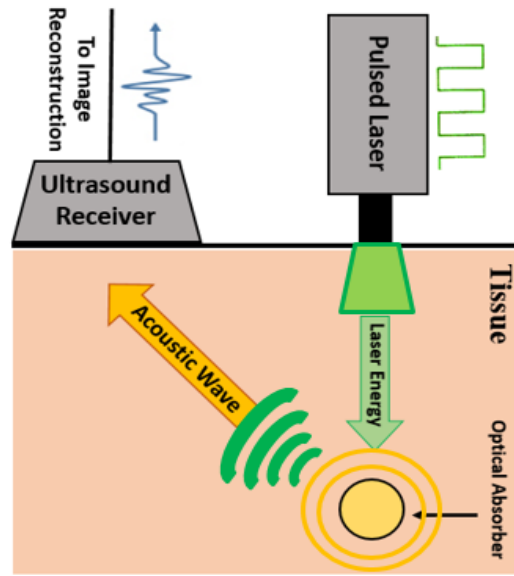


Figure 1.8: Illustration of photoacoustic (PA) signal generation in tissue. The amplitude of the PA signal is related to the optical fluence inside the tissue.

1.4.1. Photoacoustic microscopy of vascular hemodynamics

Noninvasive imaging techniques such as PAI, simplify the ability to perform longitudinal studies and are needed to track brain function throughout disease progression [89]. PAI techniques have overcome the effects of light scattering from the scalp and skull, thus producing high resolution images of the *in vivo* mouse brain [90]. Furthermore, PA contrast is related to optical absorption which allows PA methods to noninvasively access blood oxygenation in single blood vessels by exploiting the oxygen-dependent absorption properties of hemoglobin [89], [91]. Stein *et al.* tracked the real-time oxygenation dynamics of selected vessels and demonstrated the ability of PAM to noninvasively evaluate the

oxygen status of brain vessels and create the foundation for noninvasive imaging of brain activity via the hemodynamic response [89]. As interest in imaging blood oxygenation has increased, researchers developed two classes of PA imaging: photoacoustic microscopy (PAM) that includes optical-resolution (OR) and acoustic resolution (AR) and photoacoustic computed tomography (PACT).

1.4.2. Photoacoustic microscopy versus photoacoustic computed tomography

PA neuroimaging systems can be classified into two major implementations: one based on photoacoustic microscopy (PAM) which is designed for high-resolution (1-50 μm) imaging over a superficial depth and the other is based on photoacoustic computed tomography (PACT) that is designed for deeper imaging depth with compromised spatial resolution (50-200 μm) [78]. PAM can be divided into two groups: optical-resolution PAM (OR-PAM) and acoustic-resolution (AR-PAM). OR-PAM depends on ballistic photons and therefore the imaging depth is less than 1 mm in the brain. In the contrary, AR-PAM relies on diffusive light and thus the imaging depth is determined by the penetration depth of the excitation wavelength that varies from 1 mm (blue to green light) to few mm (red to NIR light) [78]. Figure 1.9 below is an illustration of the two groups of PAM.

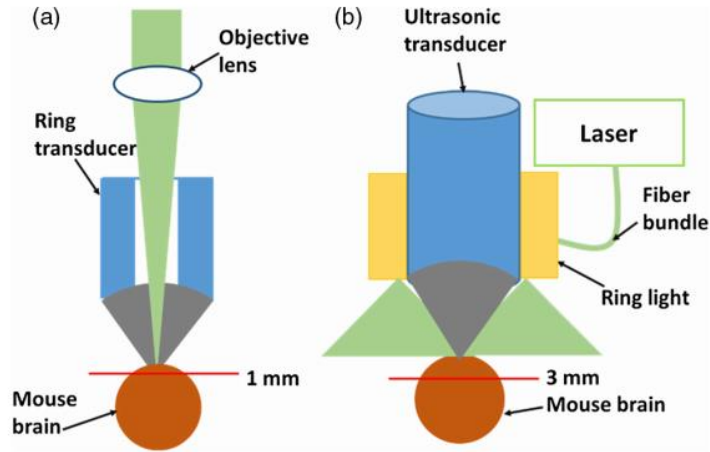


Figure 1.9: Schematics of OR-PAM (A) and AR-PAM (B) [78].

Similar to AR-PAM, PACT depends on diffusive light to generate the PA signals; however, PACT uses unfocused ultrasound transducers and thus requires computed tomography algorithms for image formation [78]. PACT can be divided into five categories: cylindrical-view PACT [92], planar-view PACT [93], and spherical-view PACT [94] where unfocused transducers are distributed on the scanning surface and 3D images can be formed (see Figure 1.10 to differentiated between the first three geometries).

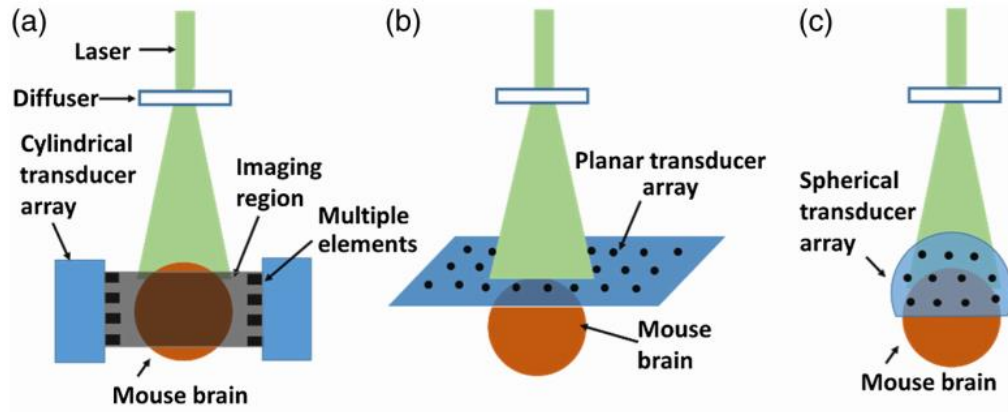


Figure 1.10: Illustrations of cylindrical-view PACT (A); planar-view PACT (B) and spherical-view PACT (C) [78].

The latter two categories - that have a 2D detection coverage and a challenging image reconstruction - are: linear-view PACT [95] and circular-view PACT [96]. Since linear and circular arrays are cylindrically focused on the 2D detection plane, scientists use the 3CCD reconstruction algorithm in their 2D systems. 3D PACT geometries are used in volumetric neuroimaging [94] and 2D PACT geometries are used for coronal- (Figure 1.11A) or transverse-view (Figure 1.11B) neuroimaging [78].

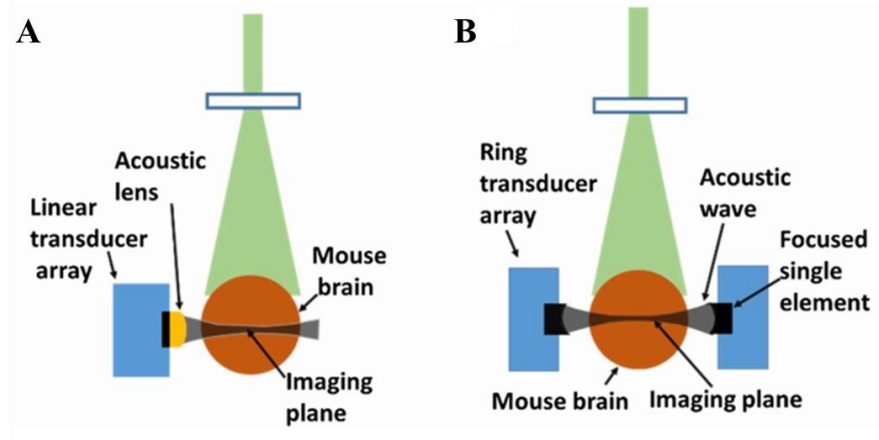


Figure 1.11: Schematics of linear-view PACT (A) and circular-view PACT (B) [78].

Non-invasive imaging of neuro-electric activity of neural populations distributed over the entire brains has been an ongoing goal of neuroscience. In the last 3 years, scientists have designed and developed real-time PA neuroimaging techniques for the visualization of neural activation deep in scattering brains using calcium-sensitive [79], [97], [98] and voltage-sensitive probes [88], [99].

1.4.3. PA measurements with calcium-sensitive dyes (CaSDs)

Recent advancement of PA neuroimaging is the visualization of neuro-electric activity using calcium-sensitive probes [79], [97], [98]. Dana, N. et al. demonstrated proof-of-concept for contrast-enhanced PAI using Arsenazo III (Asz) Ca^{2+} chelating dye to visualize cardiac myocyte depolarization *in vitro* [79]. Despite their successful demonstration of PA sensing of calcium dynamics with cytosolic Asz dye, it is known that the Asz dye binds to cellular proteins and produces free radicals that could affect cell viability [79]. Mishra, A. et al. engineered the first reversible near-infrared (NIR) Ca^{2+}

sensing probe for PAI [97]. Dean-Ben, L. X et al. were the first to examine and demonstrate the PA signature of genetically encoded calcium indicators (GECIs) by showing that the changes in GCaMP5G fluorescence are directly related to their PA signature [98]. Although, PA neuroimaging using calcium-sensing dyes are very promising, calcium imaging has its limitation and cannot substitute voltage imaging [100]. Figure 1.12 below includes the most recent PA neuroimaging using calcium-sensitive dye.

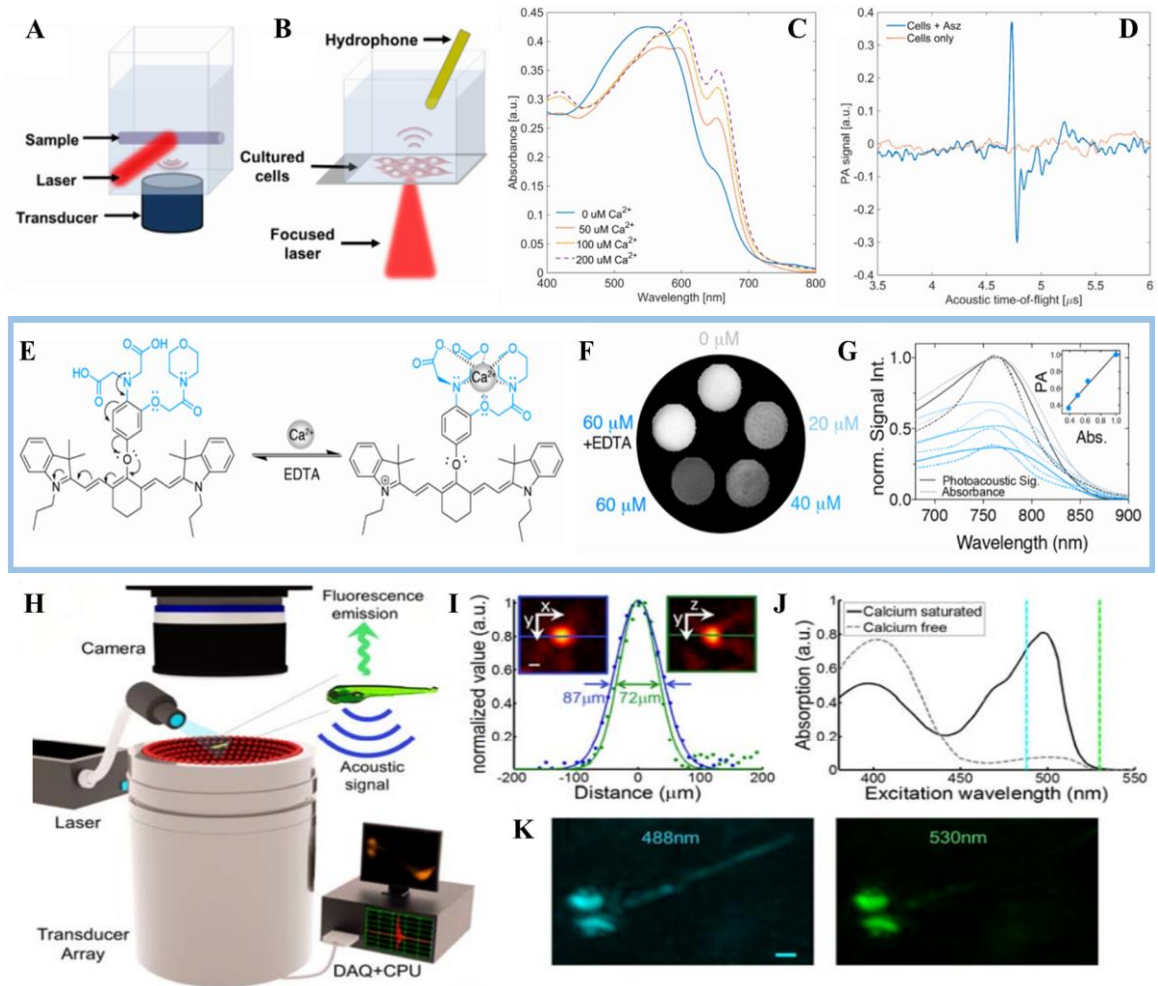
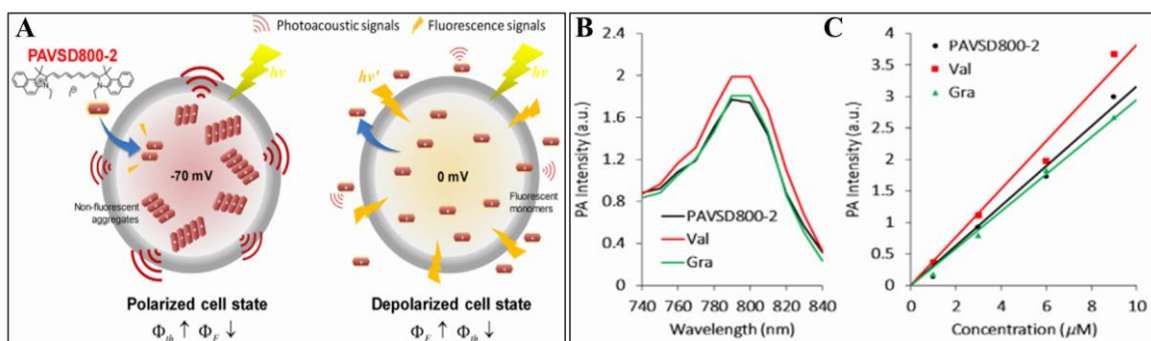


Figure 1.12: PA neuroimaging using calcium-sensitive probes. (A) Diagram of phantom imaging setup with air-beam laser irradiation and immersion transducer; (B) Modified cell-study setup with focused laser and hydrophone; (C) Absorbance of 50 μM Asz dye in buffered saline with varied Ca^{2+} concentration; (D) Photoacoustic signal of Asz-treated cells and control cells [79]. (E) Schematic representation of NIR Ca^{2+} sensing PAI probe, L, in its unbound and Ca^{2+} -bound form; (F) PA signal changes of L for varying Ca^{2+} concentrations and its reversibility upon addition of Ethylenediaminetetraacetic acid (EDTA); (G) PA spectra (solid lines) extracted from the average pixel intensities of circular region of interests covering the samples on the PA images are plotted with the absorbance spectra (dashed lines) obtained for each of the Ca^{2+} concentration. The inset shows the correlation between the absorbance and PA peak values [97]. (H) The functional optoacoustic neuro-tomography (FONT) setup; (I) Characterization of the spatial resolution of the volumetric optoacoustic imaging system was done by analyzing 3D optoacoustic images from an absorbing sphere (shown as insets with scale bar of 50 μm); (J) Spectral dependence of the absorbance on Ca^{2+} -bound versus Ca^{2+} free GCaMP5G; (K) Optoacoustic images of a 6-day old *HuC: GCaMP5G* larva acquired at 488 nm and 530 nm (GCaMP5G is barely absorbing at 530 nm; therefore, neural tissue is much more visible at 488 nm (scale bar 250 μm) [98].

1.4.4. PA measurements with voltage-sensitive probes (VSDs)

More recent studies demonstrated photoacoustic voltage response imaging methods that open up feasible technical paths for deep brain studies in the future [88], [99]. Zhang H. K. *et al.* reported a concept for designing a NIR photoacoustic VSD (PAVSD800-2) whose PA intensity change is sensitive to membrane potential and they showed that voltage-dependent quenching of dye fluorescence leads to a reciprocal enhancement of PA intensity [99]. Rao B. *et al.* reported the first demonstration of photoacoustic voltage

imaging in *in vitro* HEK-293 cell cultures and *in vivo* on the surface of murine brain using a non-radiative voltage sensor named dipicrylamine (DPA) [88]. DPA serves as a voltage-sensing acceptor that trans-locates across the cell membrane depending on the electric field [11]. Though successful at imaging bioelectric activity, Rao et al. noted that DPA does not allow sensing and imaging of voltage activity past the superficial surface layer due to short-excitation wavelength of DPA [88].



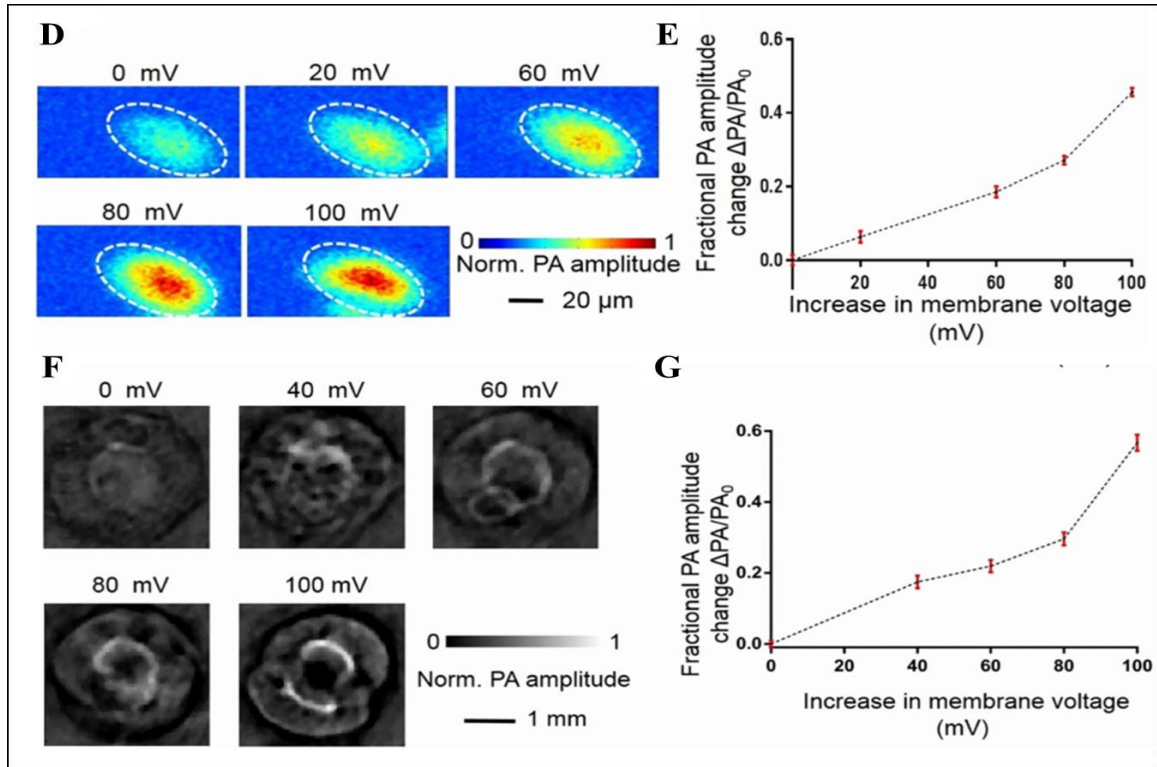


Figure 1.13: PA neuroimaging using voltage-sensitive probes. (A) The principle of the fluorescence quenching effect on the developed VSD (PAVSD800-2) according to a varying membrane potential (-70 and 0 mV in the polarized/depolarized states of neurons, respectively); (B) PA spectra of PAVSD800-2 of pre-stimulus (black) and stimulated polarized state (red) using valinomycin (Val) and depolarized (green) states using gramicidin (Gra); (C) Voltage-dependent PA intensity at 800 nm wavelength for different concentrations [99]. (D) PA maximum-amplitude projection images of HEK-293 cells demonstrate PA signal changes due to cell membrane voltage changes; (E) Fractional PA signal change versus cell membrane resting voltage changes; (F) PA images of HEK-293 cell clusters acquired through 4.5 mm thick brain tissue in response to cell membrane voltage changes; (G) Fractional PA signal change versus cell membrane voltage change [88].

Noninvasive mapping of neuro-electrical activity and cell-specific labeling, particularly in deep tissue, are critically needed to further elucidate neuronal biophysics and signaling [100]. Because PAS relies on absorption of light, a VSD that exhibits a change in optical absorption in response to a change in cell-membrane voltage is necessary for PA-based sensing of voltage. Furthermore, these probes need to provide an adequate response time (temporal resolution) to capture millisecond events associated with neuronal activity with sufficient sensitivity [101]. Development of voltage-sensitive probes that are specifically optimized for *in vivo* photoacoustic imaging and sensing is actively being pursued [99], [101].

In this research work, we developed experimental protocols that can be employed for characterizing the voltage-dependent optical response of voltage-sensitive probes and demonstrated the feasibility of PA voltage-based sensing of bio-electrical activity.

CHAPTER TWO: MATERIALS AND METHODS

In the present study, the photoacoustic sensing (PAS) of voltage-sensitive probes and the proof-of-concept were done *in vitro*. A bench-top methodologies were developed: (1) to characterize the optical-absorption properties of various voltage-sensing indicators and determine the optimal probes for PAS and (2) to demonstrate the feasibility of PA voltage-based sensing and monitoring of changes in cell-membrane potential. Labeled PC12 cells and duck-fat layers were used as simple systems to be chemically and electrically depolarized, respectively. In the following sections, a detailed discussion of the materials and methods that were used for the experimental setups and data collection will be presented.

2.1. PC12 cell culture

PC12 is a cell line derived from pheochromocytoma of the rat adrenal medulla [102], [103], that has an embryonic origin from the neural crest that has a mixture of neuroblastic and eosinophilic cells [104]. PC12 cells possess large dense core vesicles (LDCV) that contain catecholamine (the majority of catecholamine contained in PC12 cells is dopamine). These LDCVs in PC12 cells are slightly smaller (150-240 nm diameter) compared with chromaffin cells (340 nm diameter) [105]. The release of catecholamines from PC12 cells leads to amperometric spike similar to the spikes observed for isolated chromaffin cells [105], [106]. PC12 cell line has been the most used and cited culture for neurodegeneration studies [107]. PC12 cell line has many attractive properties that makes it an uncomplicated and convenient *in vitro* model for various applications [107].

Furthermore, PC12 cells have a notable feature of responding to nerve growth factor (NGF) in which they are converted from proliferating chromaffin-like cells to nondividing sympathetic-neuron-like cells that extend their axons and become electrically excitable [108], [109]. Besides their attractive features, PC12 cells – as with all models – have their limitations and any results obtained with this tumor cell line does not assure that the same finding will hold on *in vivo* models [107].

Therefore, PC12 cells were chosen for our experimental studies because they are robust and easy to culture, and their lipid bilayer have been used in prior studies to investigate cell-membrane potentials [104], [110]–[113]. Research has shown that pre-treatment of cell culture surfaces improves cell growth, adhesion, morphology, migration and increases their life-span [114]. To establish a good surface adhesion of PC12 cells and improve their ability to attach to culture plates, the custom-made wells (i.e. functionalized the surface) [103], [115] were pre-coated with poly-D-lysine (PDL), a positively charged extracellular polymer [103] for ~ 12 hours. After incubating the wells with PDL for ~ 12 hours, I removed the PDL and washed the wells 3 times with 1X Phosphate-Buffered Saline (PBS), 15 minutes each time. Cells were grown on a PDL (50 µg/mL) matrix and maintained in RPMI media (ATCC) supplemented with 10% horse serum, 5% fetal bovine serum, and 1% Penicillin Streptomycin (Thermo Fisher, Waltham, MA, USA) [116]. The cells were maintained at 37⁰C in an atmosphere containing 5% CO₂. The cells were stained for 10-15 minutes with commercially available VSDs (RH795, RH155 and indocyanine green (ICG)) dissolved in cell media and/or with voltage-sensing QD construct, based on previously published work [59], [117].

2.2. Methods to induce a change in membrane-potential

Two chemicals were used to monitor the change in membrane potential, by the administration of known concentrations of potassium chloride (KCl) and sodium tetraphenylborate (TPB).

2.2.1. Potassium chloride (KCl)

A stock solution of 0.1 M potassium chloride (KCl) was prepared in deionized water. Cell-membrane depolarization was chemically induced by adding 1.25, 2.5, 5 and/or 10 μ L of the KCl stock solution to 500 μ L total volume of cell culture resulting in added KCl concentrations of 2.5, 5, 10 or 20 mM, respectively. These concentrations were chosen because 1) they produced a detectable change in membrane potential of the PC12 cells, 2) they do not cause any deleterious effects to the cells, and 3) are within the range of ion flux that is consistent with *in vivo* conditions. All experimental measurements were performed within 24-72 hours after plating at room temperature.

2.2.2. Tetraphenylborate (TPB)

Changes in the optical properties of VSDs such as RH795 in response to changes in cell-membrane potential were studied by adding a solution of sodium tetraphenylborate (TPB), which is known to induce a change in cell-membrane potential [13], to the labeled PC12 cells. TPB binds at a short distance from the water-membrane interface and produces strong membrane electric fields [13], which can alter the optical properties of voltage sensitive dyes such as RH795 [14]. A 0.01M stock solution of TPB (sodium tetraphenylborate, Sigma Aldrich, MO, USA) was prepared in ethanol. For measurements with cell culture, 5 μ L of the stock solution was added to 500 μ L of culture to give a final

TPB concentration of 100 μ M. For absorbance measurements, the effect of the small volume of ethanol added on the spectrum of the membrane-bound dye RH795 was checked in separate control experiments and found to be negligible under the experimental conditions used. Hence, the final solutions contained a small and constant percentage of 1.0% ethanol and such a small concentration of ethanol is not expected to perturb the membrane structure significantly[13], [118].

2.3. Voltage-sensitive dyes and probes

To test and study the feasibility of using VSDs with PA sensing to measure bio-electrical activity, several commercially available dyes such as the conventional fluorescence VSD RH795 [119], [120], the absorption VSD RH155 [59], [121], and ICG VSD [122] were purchased. In addition, a novel voltage-sensing quantum dots (QDs) [117] were provided by our collaborator at Naval Research Laboratory (NRL), Dr. James Delehanty. In this section, the followed procedure(s) for cellular labeling with these voltage-sensitive dyes/probes will be presented.

2.3.1. RH795 dye preparation and cell-labeling

The styryl dye RH795 (Pyridinium, 4-[4-[4-(diethylamino) phenyl]-1, 3-butadienyl]-1-[2-hydroxy-3-[(2-hydroxyethyl) dimethylammonio] propyl]-, dibromide/172807-13-5; Biotium, Hayward, CA) was used without further purification. An 8.5 mM stock solution of the hydrophilic dye RH795 was prepared by diluting 5 mg dye in 1 mL of methanol. The aliquots of the stock solution were kept in darkness at -20°C. For bath application, the stock solution was diluted in cell media the final concentration of

0.5 mM for dye testing. Figure 2.1 below shows standard optical microscopy image and fluorescence image of the PC12 cells with extracellular RH795 staining.

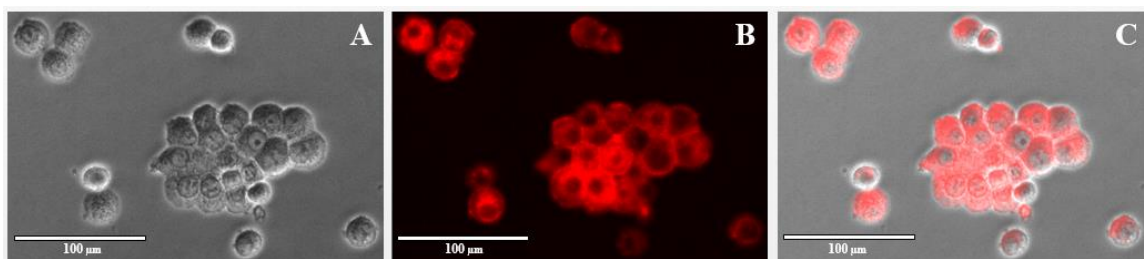


Figure 2.1: Staining of live intact rat PC12 pheochromocytoma cells with RH795 styryl VSD: (A) Live view of the cells. (B) Extracellular staining of cells with RH795 VSD. (C) Merge of A and B. (scale bar 100 μm).

2.3.2. RH155 dye preparation and cell-labeling

The oxonol neurodye RH155 of $950.26 \text{ g mol}^{-1}$ molecular weight (Santa Cruz Biotechnology Inc., Dallas, TX) was used without further purification. A 26.3 mM (25 mg/ml) stock solution of RH155 was prepared by diluting 25 mg of dye in 1 mL of deionized water. The aliquots of the stock solution were stored in darkness at -20°C . For bath-application, the stock solution was diluted in cell media to the final concentration of 100 μM . The cells staining time and protocol as well as RH155 dye preparation and concentration were based on Parsons T.D. et al. [59].

2.3.3. Cellular labeling with QD voltage-sensing probes

The QD-peptide-fullerene bioconjugate consists of a CdSe QD (electron donor) that is 8.4 nm in diameter attached to a peptide conjugate JBD1-C₆₀ that was designed and constructed by Nag O. et al. [117]. When excited in the visible regime, these QDs produce a strong emission at 605-nm. The QDs are conjugated to multiple copies of JBD1 peptides each with a fullerene (C₆₀, electron acceptor) at the end (see Figure 4.1 in Chapter 4). Based on Nag O. et al. [117], the complete growth medium was removed from the cell monolayers, and the cells were labeled with solutions of QD-peptide-C₆₀ complexes (20 nM QD appended with 20 peptides/QD; 400 nM peptide concentration) and were incubated for 10-15 minutes at 37°C followed by washing with the complete growth medium.

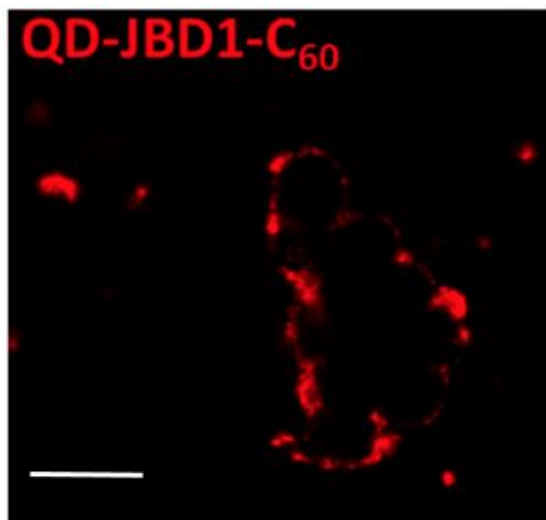


Figure 2.2: An image of PC12 cells labeled with the QD construct. Scale bar 20 μ m.

2.4. The optical-absorption characterization setup

A custom-designed optical-absorption spectrophotometer comprising of a broadband light source (AvaLight-HAL, Avantes BV, Apeldoorn, Netherlands), a spectrometer (AvaSpec-Fast, Avantes BV, Apeldoorn, Netherlands) and an integrating sphere (IS200, Thorlabs, NJ, USA) was assembled and controlled using Avasoft 8 user interface. The cells were plated on glass slides and mounted on top of the integrating sphere (see Figure 2.3). Cell-membrane depolarization was chemically induced by administering KCl in varying concentrations (2.5, 5, 10, and 20 mM). For demonstrative purposes, we employed this setup to characterize voltage dependent changes in the absorption spectra of RH155 oxonol dye.

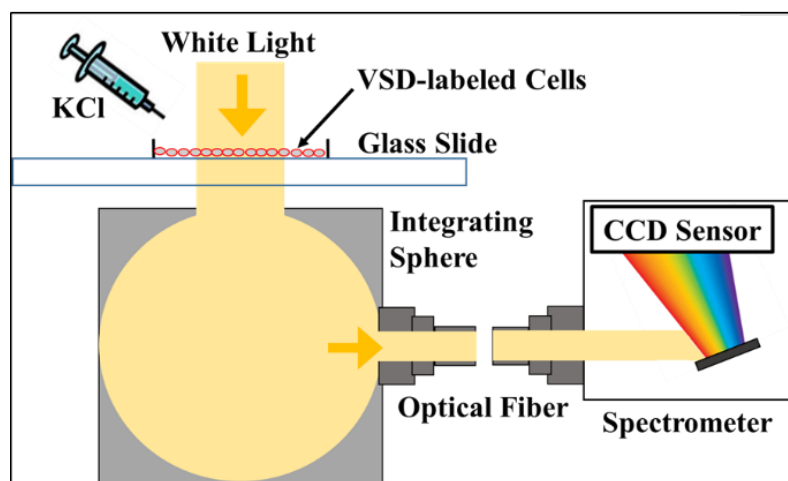


Figure 2.3: Schematic of experimental setup used to characterize optical-absorption of PC12 cells labeled with voltage-sensitive probes.

2.5. The photoacoustic signal measurement setup

To measure the photoacoustic signal of the VSD-labeled cells, a custom photoacoustic sensing setup (Figure 2.4) was developed that comprised of a 690-nm or/and 532-nm pulsed laser/optical parametric oscillator (OPO) (Phocus Mobile, Opotek, Inc., Carlsbad, CA) operating at a pulse-repetition rate of 10 Hz and a 20-MHz broadband ultrasound (US) transducer (Sonic Concepts, Bothell, WA). The OPO provided 5-ns laser pulses over wavelengths from 690 to 950 nm. Because the absorption peak of RH155-tagged cells was determined to be at 665 nm (Figure 3.4), 690-nm wavelength was chosen to excite the photoacoustic response and 532-nm wavelength was used for the PA measurements with the voltage-sensitive QDs (Figure 4.2). Laser was operated at 15 mJ/pulse, which resulted in an optical fluence of 5 mJ/cm². A fluid-filled coupling cone attached to the transducer ensured proper acoustic coupling between the transducer and the cell culture. The transducer had a focal length of 65 mm (distance between the cells and the transducer) and a full-width half maximum focal-beam waist of approximately 1.5 mm. The signal from the transducer was amplified using a low-noise 20-dB amplifier and digitized using a 12-bit digitizer.

Voltage-induced change in the PA signal of the RH155-labeled cells was investigated by administering KCl for a range of concentrations, and the patch-clamp-verified theoretical model was employed to convert the KCl concentration into voltage similar to Rao et al. [43]. The temporal dynamics of change in cell-membrane potential was also investigated by adding 2.5 mM of KCl. The PA signal (averaged 10 times) was recorded at intervals of 10 seconds for a total duration of 5 minutes. Baseline PA signal

was recorded for approximately 50 seconds prior to KCl-induced change in cell-membrane potential. The time-dependent fractional change in the PA signal was compared against the theoretically modeled change in cell-membrane potential.

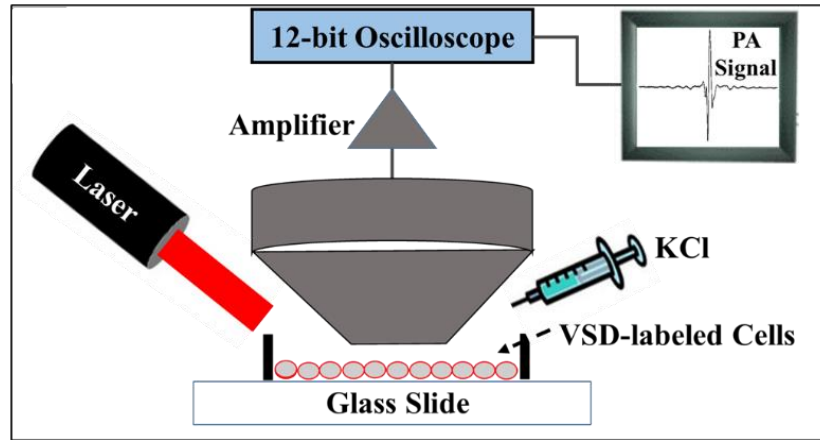


Figure 2.4: Schematic of experimental setup used to characterize PA response from PC12 cells labeled with voltage-sensitive probes.

2.6. Theoretical model

The depolarizing effects of extracellular potassium are often calculated using a Nernst potential based on assumed internal and external ionic concentrations [88]. The change in membrane potential (ΔE) is roughly estimated based on the given equation ($\Delta E = (\frac{RT}{F})\ln(\frac{Ka}{Ki})$), where R is the gas constant, T is the absolute temperature, F is the Faraday constant, Ka is the adjusted concentration and Ki is the initial concentration [88]. To better assess the effects on transmembrane potential due to changes in extracellular

potassium concentrations, a computational model was utilized along with current clamp whole-cell patch measurements. The model [123] incorporates standard Hodgkin-Huxley reversal potentials and gating variables with the addition of electrogenic pumps, a potassium and chloride cotransporter and ionic diffusion. A steady resting potential requires potassium, sodium and chloride dynamics described below. The undifferentiated PC12 cells used in our experiments i.e. not being exposed to neuron growth factor (NGF), needed to express voltage sensitive channels. Therefore, the model only includes voltage independent conductances. The membrane voltage follows:

$$C \frac{dV}{dt} = (-I_{Na} - I_K - I_{Cl} - I_P)$$

The final term on the right-hand side I_P is for the electrogenic nature of the sodium potassium pump, modeled here as:

$$I_P = \frac{P_{max}K_O}{\left(1.0 + \left(\frac{24.0mM}{Na_i}\right)^{1.5}\right)(K_O + 1.5mM)}.$$

The membrane currents are modeled as leak currents: $I_{ion} = g_{ion}(V - V_{ion})$. The average input impedance was 115 $M\Omega$ for patch clamp experiments. The model cells are assumed spherical with a radius in the range of 7.0 μm , and together with the impedance corresponds to a total membrane conductance of approximately 1.3 mS/cm^2 . Concentrations for the bathing media and internal patch-clamp solutions were matched in the model to the experimental conditions, for either patch clamping in artificial cerebrospinal fluid, or photoacoustic measurements in media. See Table 1 below.

Table 1: Parameters in the model and experimental PA measurements.

Parameter	Patch Clamp	Photoacoustics
g_k	0.5 mS/cm ²	0.5 mS/cm ²
g_{Na}	0.4 mS/cm ²	0.4 mS/cm ²
g_{Cl}	0.4 mS/cm ²	0.4 mS/cm ²
[K] _o	2.8 mM	4.48 mM
[Cl] _o	133 mM	91.4 mM
[Na] _i	130 mM	111 mM
P_{max}	0.73 mA/cm ²	0.73 mA/cm ²
Electrode Concentrations	K (130 mM), Na (3 mM), Cl (6 mM)	K (130 mM), Na (3 mM), Cl (6 mM)
k_{cc}	0.016 mA/cm ²	0.016 mA/cm ²
Δx	0.1 cm	0.1 cm
Δx_e	0.0005 cm	0.0005 cm
Δx_o	0.001 cm	0.001 cm

The average resting potential measured for a patched cell was close to -50 mV. In the model this potential was achieved by tuning the ratio of the conductances to $g_K = 0.5 \text{ mS/cm}^2$, $g_{Na} = 0.4 \text{ mS/cm}^2$, and $g_{Cl} = 0.4 \text{ mS/cm}^2$. The individual reversal potentials were calculated using the standard Nernst potential $V_{ion} = 26.64 \text{ mV} \ln(\frac{C_{out}}{C_{in}})$, and the ionic concentrations for the intracellular and extracellular spaces are modeled by the following dynamics:

$$\tau \frac{dK_o}{dt} = \beta_1(I_K + I_{KCC1} - 2I_P - I_{K,O})$$

$$\tau \frac{dK_i}{dt} = \beta_2(-I_K - I_{KCC1} + 2I_P - I_{K,I})$$

$$\tau \frac{dNa_o}{dt} = \beta_1(I_{Na} + 3I_P)$$

$$\tau \frac{dNa_i}{dt} = \beta_2(-I_{Na} - 3I_P - I_{Na,I})$$

$$\tau \frac{dCl_o}{dt} = \beta_1(-I_{Cl} + I_{KCC1} - I_{Cl,O})$$

$$\tau \frac{dCl_i}{dt} = \beta_2(I_{Cl} - I_{KCC1} - I_{Cl,I})$$

The cotransporter for potassium and chloride is modeled as $I_{KCC1} = kcc \cdot \log\left(\frac{K_i Cl_i}{K_o Cl_o}\right)$, and is required to balance the ionic dynamics [124].

In our experiments the extracellular potassium chloride concentration was elevated by injecting a small amount of high concentration solution approximately 5 mm from the location of observation, either the patched cell or the center of the photoacoustic target. To model the time course of the concentrations in the dish a simple diffusion model was utilized:

$$\frac{\Delta C_x}{\Delta t} = D \left(\frac{C_{x+1} - 2C_x + C_{x-1}}{\Delta x^2} \right) + D \left(\frac{C_{y+1} - 2C_y + C_{y-1}}{\Delta x^2} \right)$$

The diffusion constant for all ions was set to $D=2.7 \times 10^{-5} \text{ cm}^2/\text{sec}$. The bath concentration affected the local ionic concentrations K_o and Cl_o through $I_{ion,O} = D \frac{(C_{ion,Bath} - C_{ion,o})}{\Delta x_o^2}$. The factors β_1 and β_2 are conversion factors between electrical and concentration currents and differ by the relative volume of the internal and external spaces. For these experiments the external space is assumed to be significantly larger than the internal and the diffusion with the local bath dominates the external concentration. The intracellular term, $I_{ion,I} = D \frac{(C_{ion,i} - C_{ion,e})}{\Delta x_e^2}$ is only used when modeling diffusion with the patch electrode and essentially fixes the internal concentrations of the cell to those of the electrode.

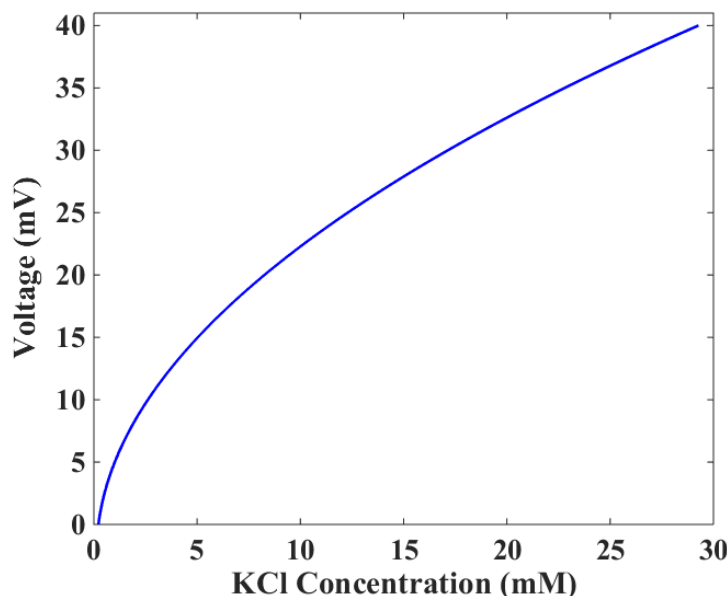


Figure 2.5: KCl concentration conversion into change in membrane potential (mV).

2.7. Patch-clamp recording setup

The glass slides with PC12 cells were mounted on an optical-fluorescence microscope. Whole-cell current-clamp recordings were performed in conventional patch-clamp mode [125], [126] with an Axopatch 200B amplifier (Molecular Devices, Sunnyvale, CA, USA). The recording electrodes were pulled from borosilicate glass (2 mm outer diameter (OD), 0.75 mm inner diameter) by a two-stage horizontal puller and had a resistance of $\sim 8 \text{ M}\Omega$ when filled with internal solution containing 140 mM potassium gluconate, 1 mM CaCl_2 , 11 mM EGTA, 2 mM MgCl_2 , 3 mM NaATP, and 10 mM HEPES. Voltages were recorded and data were analyzed off-line using pClamp 6.03 software (Axon Instruments, Foster City, CA, USA).

As a calibration step, the PL-response of the QD-bioconjugates was cross-validated and calibrated using the whole-cell patch clamp setup that was discussed above. The patch-clamp was used to incrementally, step-wise increase the cell membrane potential of a QD-tagged PC12 cell from resting potential and hold them at a prescribed voltage while a high-sensitivity video microscope measured the QD-PL response.

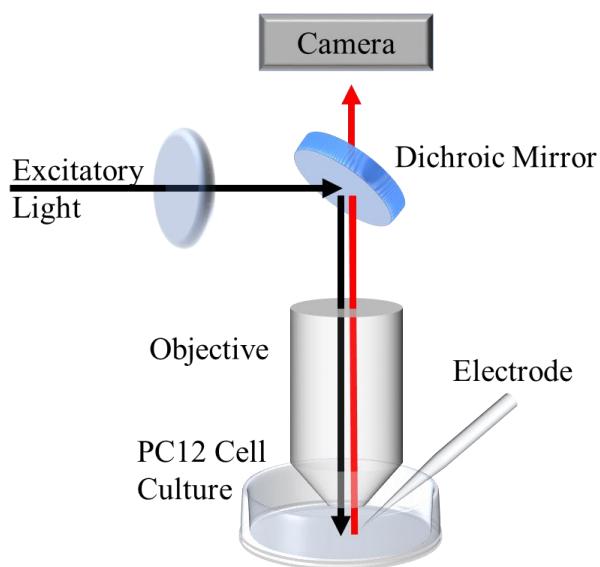


Figure 2.6: Schematic of the patch-clamp recording setup from a single PC12 cell for validation and calibrating the probe-PL signal with respect to the cell membrane potential.

CHAPTER THREE: PHOTOACOUSTIC SENSING OF BIO-ELECTRICAL ACTIVITY USING VOLTAGE-SENSITIVE DYES

Optical-fluorescence imaging provides molecular specificity and spatio-temporal resolution necessary for noninvasive imaging of cellular interactions and bio-electrical activity. However, these techniques suffer from limited imaging depth constrained by optical absorption and scattering in tissue. This study investigated the feasibility of photoacoustic sensing (PAS) of biopotentials, which relies on absorption of light by voltage-sensitive probes and subsequent generation/detection of ultrasound. Pheochromocytoma (PC12) cells were tagged with voltage-sensitive dyes, such as RH795 and RH155. Cells were depolarized by changing the extracellular potassium ion concentration (administering potassium chloride (KCl)), which was verified using whole-cell patch-clamp. A spectrophotometer was used to characterize the corresponding change in optical absorption. Absorption of light in the range of 500-900 nm decreased as the membrane potential increased. A nm-pulsed laser excited the photoacoustic (PA) response from RH155-labeled cells. PA-signal amplitude exhibited a monotonic change with increasing cell-membrane potential and the dynamics of the PA-signal change was consistent with the theoretically modelled change in membrane potential.

3.1. Optical-absorption characterization of VSD-labeled cells

The developed setup for characterizing the optical-absorption properties of the voltage-sensitive probes allows us to test the solvent(s) effects on the dyes. For instance, working with the conventional RH795 dye, we knew that different mechanisms are involved including the solvatochromic effect. Therefore, before measuring the optical absorption of the RH795-labeled cells, the effect of solvents on the absorption spectrum of RH795 dye was tested. Figure 3.1 shows the effect of the solvent on the absorption spectrum of the RH795; the dye was dissolved in methanol and buffer solutions. Results indicated that the use of different solvents to make stock and/or staining solutions of RH795 can slightly modify the overall magnitude of absorption but absorption-spectra retain the same profile.

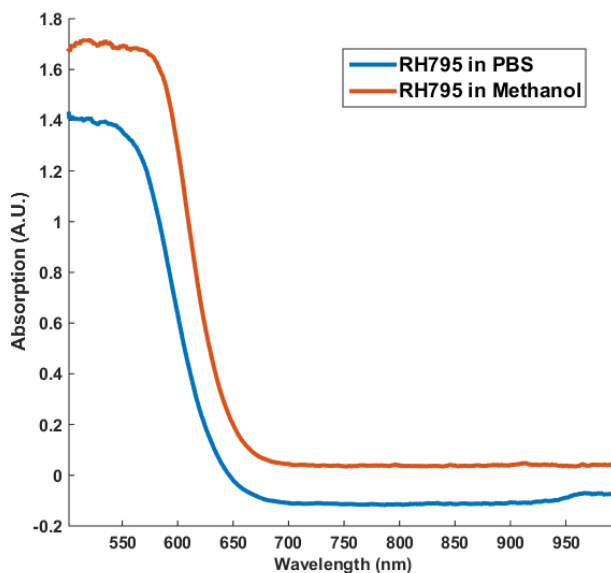


Figure 3.1: Optical absorption spectra of 0.5 mM RH795 dye in methanol (stock solution) and buffer.

Spectroscopic changes in optical absorption of VSDs such as the fluorescence RH795 dye and absorption RH155 dye as a function of TPB and KCl concentration were measured in PC12 cells, respectively. Spectroscopic characterization of changes in optical absorption of RH795 as a function of TPB-induced change in membrane potential was evaluated in PC12 cells. Figure 3.2 shows change in the absorption spectra of (3.7 μM) RH795 bound to PC12 cells resulting from addition of 100 μM TPB at room temperature. Absorption spectra recorded before and after the addition of 100 μM TPB exhibited a wavelength shift in the absorption peak (approximately 510 nm to 550 nm) as well as a decrease in the overall magnitude of absorption in the wavelength range of 500-900 nm.

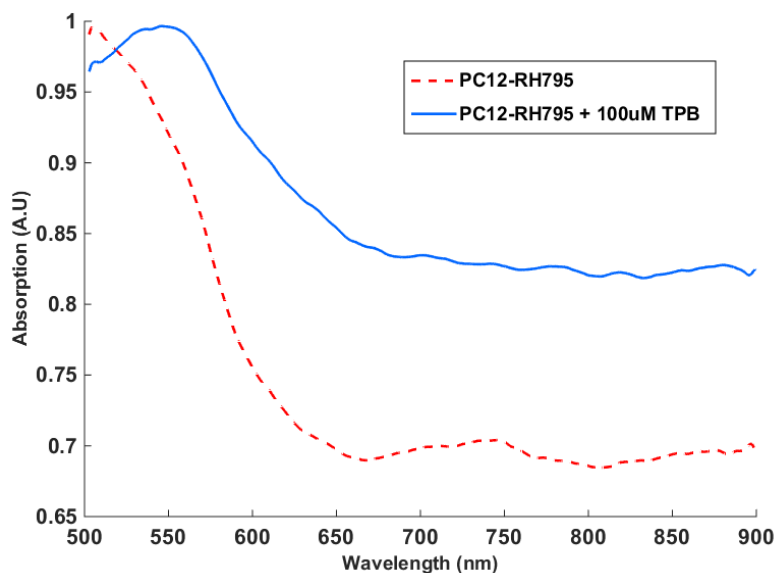


Figure 3.2: Absorption spectra of 3.7 μM RH795-labeled cells in the presence and absence of 100 μM TPB; $T=25^{\circ}\text{C}$.

Based on the results, we concluded that RH795 fluorescence dye was not an optimal dye to be used for photoacoustic sensing since its absorption spectra showed changes in the spectral amplitude as well as a wavelength shift (see Figure 3.3 below) as a function of chemical induction. The occurrence of the wavelength shift that was related to the dye's mechanisms made it hard to track the PA signal of the RH795-labeled cells. The absorption spectrum peak of the RH795-labeled cells (~ 510 nm, see Figure 3.2 above) was shifting to the right passing through 532 nm, as a function of chemical induction.

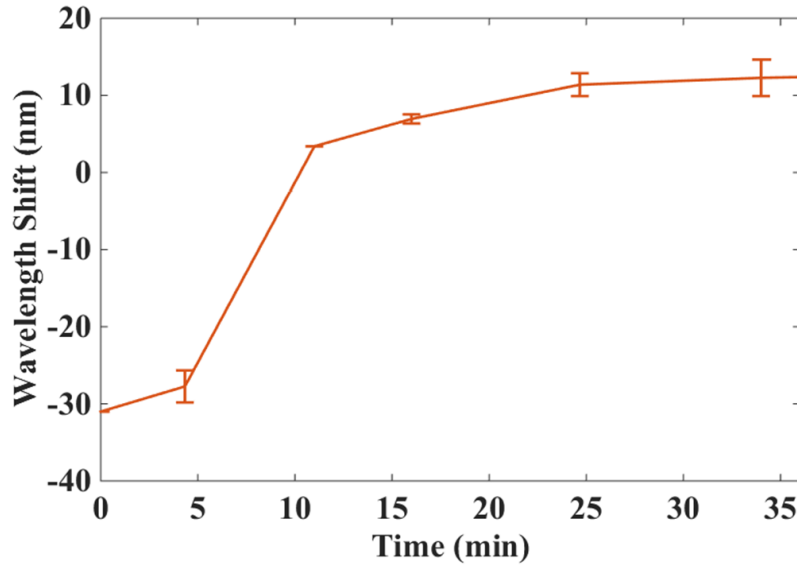


Figure 3.3: Spectral shift of RH795-labeled cells relative to 532 nm as a function of TPB. The error bars are a representation of standard deviation (N=4).

Since the work with the fluorescence VSDs such RH795 and indocyanine green (ICG) was not successful, we sought to find an absorption VSD that is commercially available and test its performance with PA sensing for visualizing electrical activity. As an initial step, the characterization of the optical-absorption

properties of the absorption dye RH155 was needed and performed. The absorption spectra (500-900 nm) decreased in magnitude after KCl was administered to the cell culture (Figure 3.4) without showing any shift in the wavelength. The optical absorption exhibited a decrease with the increase in cell membrane potential.

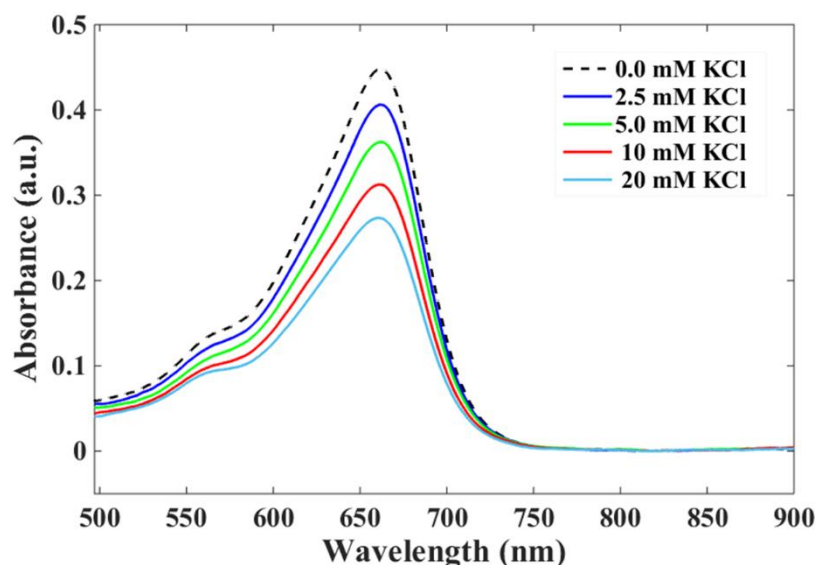


Figure 3.4: Optical-absorption spectra of RH155-labeled PC12-cells as a function of change in KCl concentrations.

The absorption spectra of each measurement were recorded for 5 minutes with 2 second integration time and at 50-second time point a specific KCl concentration was manually administered. Avasoft 8 was used for data collection. For the data analysis, mean subtraction was performed by subtracting the average between 850 and 900 nm from the whole spectrum. Then the average of the recorded data of the baseline (before the addition of KCl) was obtained and fractional change was calculated using the formula below where

A_T is the absorption at a given time stamp and A_{Avg} is the average absorption of the recorded data prior to the KCl administration.

$$\frac{\Delta A}{A} = \frac{(A_T - A_{Avg})}{A_{Avg}}$$

After characterizing the labeled cells, the absorption peak was found to be approximately 665 nm. However, our nm-pulsed laser operates in the range between 690-950 nm, so we investigated the absorption at 690 nm. Figure 3.5 shows the fractional change in absorption of the stained cells as a function of KCl concentration incorporated with the theoretical model. As the concentration of KCl increased, the absorption fractional change decreased.

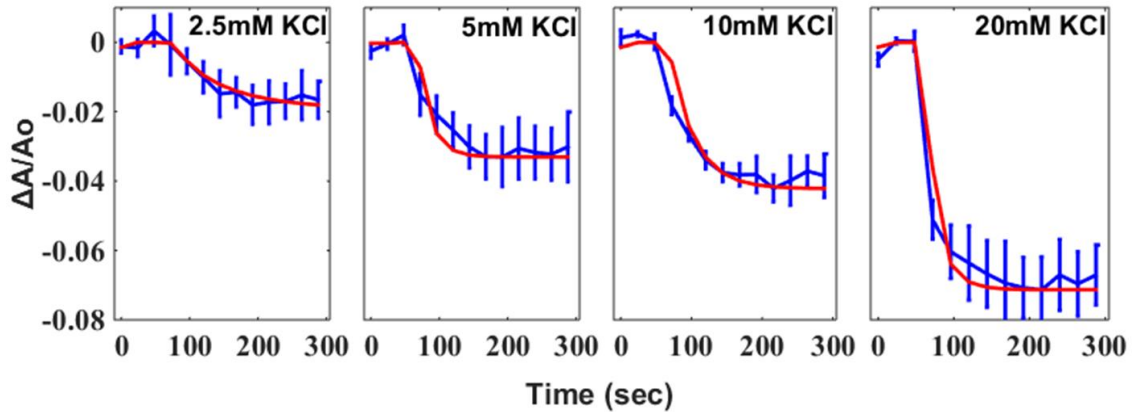


Figure 3.5: Fractional changes in optical-absorption (experimental data (in blue) versus modeled data (inverted in red)) of RH155-labeled PC12 cells at 690 nm as a function of 2.5 mM, 5 mM, 10 mM, and 20 mM KCl-induced depolarization. Error bars represent the standard deviation between multiple trials (N=4).

To study the osmolality effect, the optical-absorption properties of the labeled cells was characterized by administering sucrose with equivalent concentration of the 40 mM KCl concentration. Figure 3.6 shows the fractional change in absorption of the labeled cells as a function of time as KCl and sucrose were administered at 50 seconds time point.

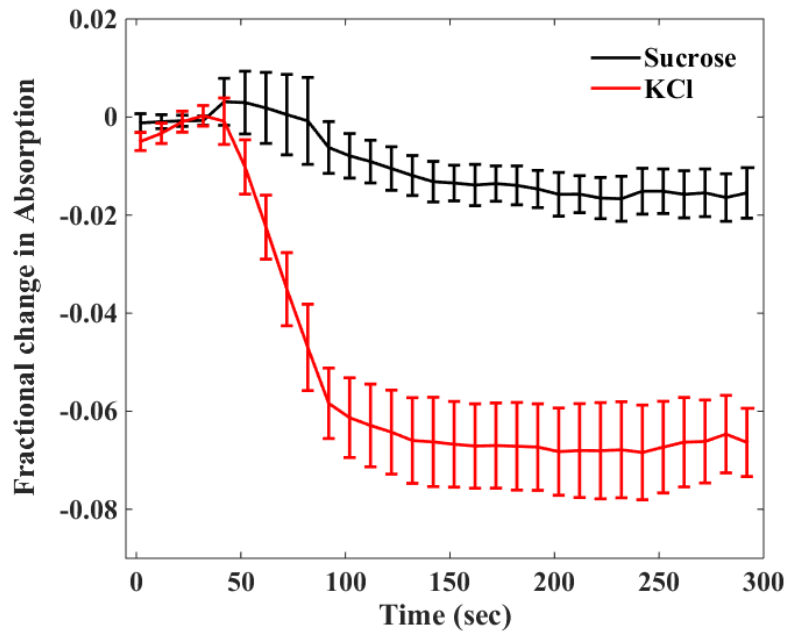


Figure 3.6: Fractional change in absorption of the RH155-labeled cells at 690 nm wavelength as a function of time as KCl and sucrose were administered. Error bars represent the standard deviation between multiple trials (N=4).

3.2. Photoacoustic signal sensing of RH155-labeled cells

After characterizing the optical-absorption spectrum of the RH795 dye, we wanted to test whether or not this fluorescence dye would produce a PA signal. Figure 3.7 below shows the PA signal of RH795-labeled cells. However, it was very hard to sense the change in membrane potential as a function of chemical induction, due to the fact that multiple mechanisms were involved in the behavior of this dye that was accompanied with spectral shift.

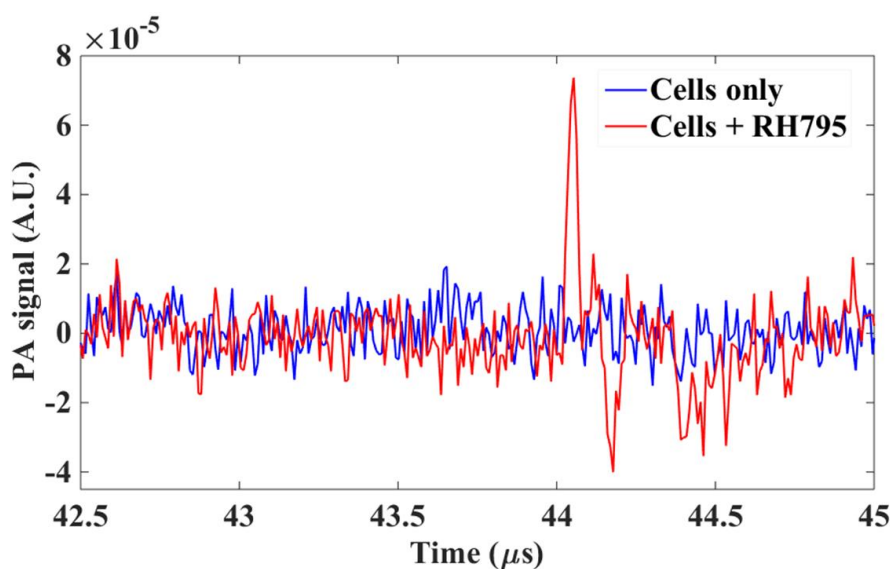


Figure 3.7: PA RF-line of RH795-labeled PC12 cells and control cells.

Although RH795 VSD produced a PA signal, we determined that this VSD was not suitable for PA sensing and/or imaging due to its spectral shifting that made it hard to track the change in membrane potential. Therefore, after characterizing the optical-absorption

properties of the RH155 absorption dye that showed a change in the amplitude of the spectrum, the feasibility of using RH155 with PA sensing was studied to determine whether or not it produces a PA signal.

As a control, the RH155 dye was dissolved in cell media and tested with the PA measurements setup that was discussed in Chapter 2 (see Figure 2.5). As to our expectation, this absorption dye produced a PA signal. Hence, we proceeded with the cellular labeling and voltage sensing. Figure 3.8 below shows the PA signals from untagged PC12 cells and the RH155-labeled cells. The labeled cells produced a PA signal that was approximately 20 times greater than the PA signal obtained from cells without RH155 dye (see Figure 3.8). The time-of-flight of the PA signal from cells was approximately 44 μ s, which was consistent with the transducer's focal length of approximately 66 mm. If we divide 65 mm (the focal length of the transducer used in our setup) by speed of sound (1.5 mm/ μ s), the result will be approximately 44 μ s. therefore, we expect that the PA signal will always appear within the 42-45 μ s window. Photo-stability of the dye for 5 mJ/cm² fluence was verified by measuring the PA-signal amplitude over a 5-minute interval; the PA-signal did not exhibit a change during this time (see Figure 3.9).

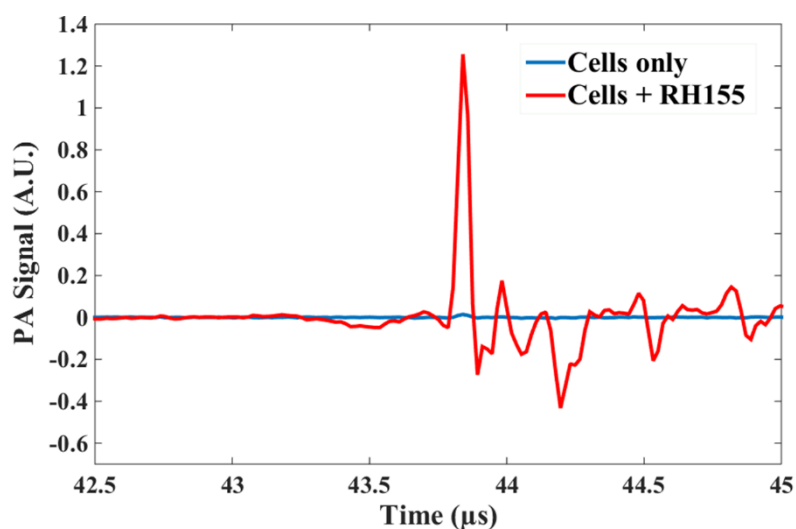


Figure 3.8: Photoacoustic (PA) signals of RH155-labeled cells and control cells.

Knowing that the RH155 produced a PA signal, its response to KCl-induced depolarization was tested. The PA experiments were designed in a similar fashion to that of the optical-absorption characterization measurements where data collection was recorded for 300 seconds while administering KCl concentration(s) at 50 seconds time point. Most VSDs are designed for fluorescence imaging suffer from photobleaching and quenching. Therefore, before every measurement the PA signal from the RH155-labeled cells was recorded without any administration of KCl (administering deionized water) and monitored the change within the time interval of my experiments. Figure 3.9 shows the fractional change in the PA signal as a function of time without KCl administration (adding a certain volume of deionized water) and with 2.5 mM KCl administration. These results showed that the PA signal of RH155 did not change and the dye was photostable and did not photobleach for the duration of the experimental measurements.

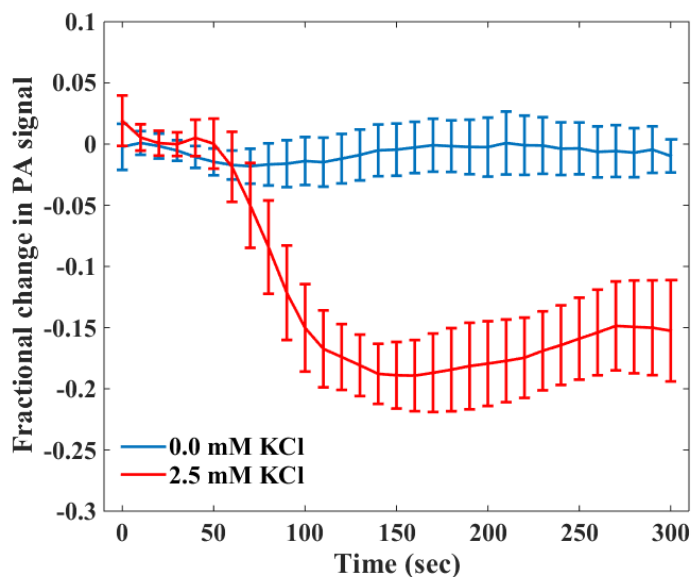


Figure 3.9: Fractional change in the PA signal of RH155-labeled cells as a function of time with the administration of 2.5 mM KCl (red) and without KCl (blue). The error bars are a representation of standard deviation. Error bars represent the standard deviation between multiple trials (N=4).

The PA signal response of the RH155-labeled cells as a function of time was tested while changing the extracellular potassium ion concentration (applying external concentrations of KCl starting with 2.5 mM, 5mM, 10 mM and ending with 30 mM). Figure 3.10 is a representation of the fractional change in the PA signal of the labeled cells as a function of time with various concentrations of KCl that was administered at 50 seconds time point.

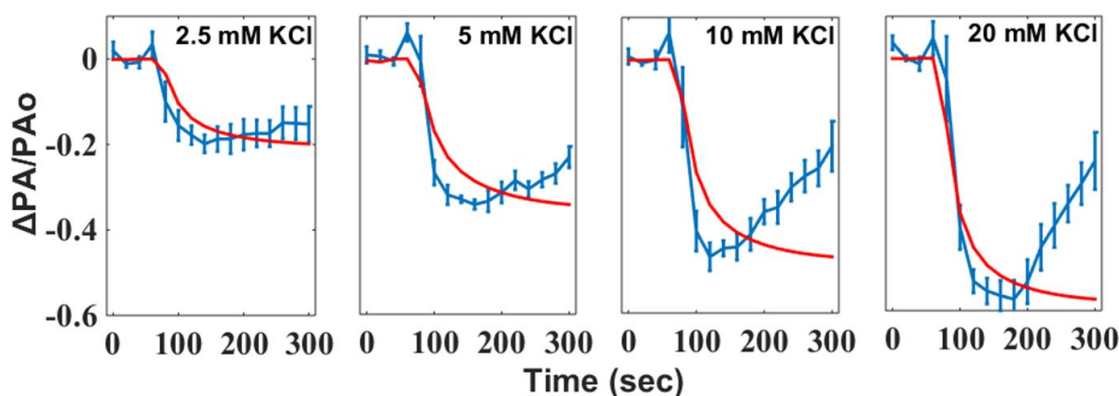


Figure 3.10: Fractional changes in PA-signal amplitude (experimental (in blue) versus theoretical model (inverted in red)) of RH155-labeled PC12 cells at 690 nm as a function of 2.5 mM, 5 mM, 10 mM, and 20 mM KCl-induced depolarization. Error bars represent the standard deviation between multiple trials (N=4).

The cells occupy a rather small fraction of the total volume of the dish. Therefore the addition of KCl to the dish changed the ionic environment around the cells for the duration of the experiment causing them to enter a new steady state with their environment. Our theoretical model was utilized to predict the new steady state of the cells. Both experiments and models show that the approach to the new steady state is long but reasonably converged by 100 seconds after the addition of KCl. The values for this time point were used to predict the depolarization induced by the addition of the KCl. Figure 3.10 above displays the time course for both the PA response as well as the model results.

To study the osmolality effect, PA sensing of the RH155-labeled cells was conducted with administering low and high concentrations of sucrose that were equivalent to the lowest and highest concentrations of KCl that was used in our experimental design i.e. 2.5 mM and 20 mM, respectively. Figure 3.11 shows the fractional change in the PA

signal of the labeled cells as a function of time as KCl and sucrose were administered at 50 seconds time point. Sucrose was added in twice the concentration of KCl in order for the same osmotic pressure to be asserted by KCl (ionic) and sucrose (nonionic) [127]. For example, KCl can dissociate in solution into K^+ and Cl^- ions; therefore, for every 1 mole of KCl in solution there are 2 osmoles of solute particles since both ions have an effect on the osmotic pressure of solution. On the other hand, sucrose does not dissociate and 1 M sucrose is a 1 osmole sucrose solution. In Figure 3.11 B, 20 mM KCl and 40 mM sucrose were administered to the RH155-labeled cells.

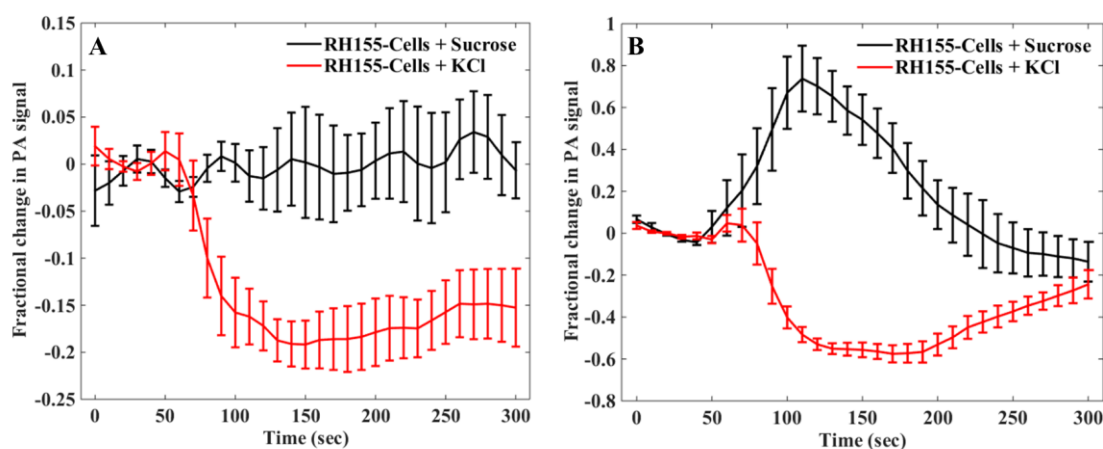


Figure 3.11: Fractional change in PA signal of RH155-labeled cells as a function of time with KCl and sucrose with low (A) and high (B) concentrations. Error bars represent the standard deviation between multiple trials (N=3 for the sucrose experiments and N=4 for the KCl experiments).

3.3. Electrophysiological recordings and theoretical model

Whole-cell patch-clamp recordings of the membrane potential were performed in the current-clamp configuration. Once patched, the PC12 cell's resting membrane was typically near -50 mV. The extracellular concentration of potassium ions was elevated by administering increasing concentrations of potassium chloride (KCl), which in turn induced a change in cell-membrane potential. Figure 3.12 shows the time-evolution in the membrane potential of a single PC12 cell after administering KCl in increasing concentrations of 4.8 and 10.8 mM. The dashed lines indicate the results from our model cell for the same two increases in extracellular potassium.

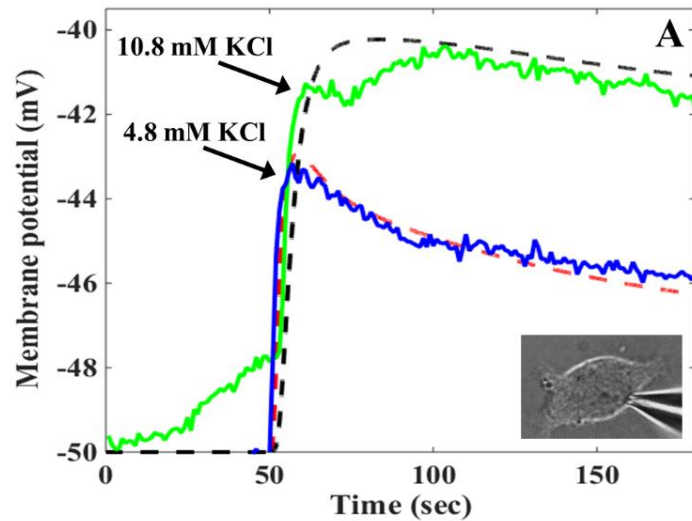


Figure 3.12: Time evolution of cell-membrane potential of a patched PC12 cell (solid lines) and calculated cell-patch model (dashed lines) as a function of 4.8 mM and 10.8 mM KCl-induced depolarization.

3.4. Discussion

In this study, we developed *in vitro* protocols to characterize and screen potential voltage-sensitive probes for photoacoustic imaging. We examined the photoacoustic signature of a commercially available VSD and demonstrated its feasibility for photoacoustically sensing changes in cell-membrane potential.

Photoacoustic sensing and imaging of voltage has the potential to address a significant need of improving imaging depth while providing resolution necessary to investigate signaling in large intact neural circuits. Although turn-key instrumentation for acquiring high-fidelity 2D and 3D photoacoustic images of rodent brain is commercially available, lack of VSDs optimized for PAS is a major hindrance. Potential VSDs should have the following characteristics to be suitable for PA-based imaging of neuro-electrical activity: (1) optical-absorption peak in the near-infrared to infrared regime for optimal penetration in tissue, (2) optical-absorption signature that exhibits a voltage-dependent change in magnitude or spectroscopic shift, and (3) temporal response in millisecond scale. We chose RH155 dye for this study because it is an absorption VSD with absorption peak centered at 650 nm and it is commercially available voltage-sensitive dye. Because photoacoustic signal relies on absorption of light and subsequent thermoelastic expansion of the medium, absorption-based dyes (usually low quantum yield, more heating) will be better suited as photoacoustic voltage reporters than conventional fluorescence-based voltage reporters (high quantum yield, less heating).

In PAS, incident optical energy is converted into sound through localized heating and the mechanism in generating acoustic signal involves absorption of optical energy,

localized heating, and subsequent thermoelastic expansion described as $p = \alpha \xi \Gamma m \mu F$ [43] that was discussed in Chapter 2. The plasma membrane potential does not change α , ξ , Γ , and F . The only likely mechanism to cause a change in m is cell shrinkage due to additional of KCl; however, the KCl concentrations employed in our study (2.5-20 mM) are similar to physiological values and significantly lower than those employed in previously published studies [43]. Therefore, cell-shrinkage is not likely the cause of change in PA signal in our study. Hence, the voltage-dependent change in PA signal observed likely resulted directly from a voltage-dependent change in optical absorption, μ . The voltage-dependent change in optical absorption measured using the custom spectrophotometer supports this conjecture. There are three primary physical mechanisms that can play a role in VSD-based measurements [11]. The first is the electrochromic effect, which involves intramolecular charge redistribution without chromophore movement, produces a shift in the absorption spectra. This was not observed in our measurements (refer to Figure 3.4 above). Based on our absorption spectra and PA signal measurements, which showed a decreasing trend as membrane-potential increased, we hypothesis that the mechanism involved with RH155 dye could be one of the two other mechanisms reported in [13]: repartitioning where the chromophore moves in or out of the cell membrane resulting in a change in the absolute dye concentration; or reorientation where the electric field produces a torque changing the relative alignment of the dye molecules with respect to the membrane.

In PA-based approach, the information from VSDs to the sensor is relayed acoustically (instead of optically), therefore, PA-based approach potentially could provide

useful sensing and mapping of bioelectric activity deeper in tissue in comparison to the sensing depths possible using fluorescence-based techniques. VSDs that have an absorption peak in the near-infrared regime will further improve sensing depth.

The current laser was limited to a pulse-repetition frequency of 10 Hz, which does not provide the temporal resolution necessary for resolving neuronal action potentials. KCl-induced “slow” changes in cell-membrane potential provides a convenient model for characterizing the performance of photoacoustic VSDs *in vitro*. *In vivo* implementation of PA-based voltage imaging will require nanosecond-pulsed lasers with a pulse repetition rate 1 kHz or greater [90], [128] in order to resolve action potentials.

3.5. Conclusion

In this study, the feasibility of PA-based voltage sensing was investigated using RH155-labeled PC12 cells that were depolarized by adding KCl. PAS can potentially alleviate challenges encountered in current fluorescence-based methods. When combined with the suitable VSDs, PAS systems could be optimized for deeper imaging of the electrical activity in the brain.

CHAPTER FOUR: QUANTUM-DOT-BASED VOLTAGE REPORTERS FOR DUAL-MODALITY SENSING OF BIOELECTRIC ACTIVITY

The measurement of electric fields in cellular biology has been limited to membrane-dependent methods such as VSDs [14], [129], [130], patch and voltage clamps, green fluorescence protein methods, or fluorescence resonance energy transfer (FRET) techniques. However, these methods are limited to $< 0.1\%$ volume fraction of the cell [63]. Therefore, the need for voltage-sensitive probes that are specifically designed for PA sensing and imaging is essential. A wide range of voltage-sensing optical probes have been designed and tested in different *in vitro* and *in vivo* systems [14], [129], [130]. As mentioned in the previous chapters, these optical techniques are limited to penetration depths of less than 1 mm [50], and therefore, are better suited for *in vitro* applications. One viable alternative to overcome the depth limitation of fluorescence-based methods is photoacoustic (PA) sensing. The PA-based methods provide spectroscopic specificity to endogenous and exogenous chromophores, but the molecular information is relayed to the sensor acoustically, which is not as susceptible to scattering in tissue as light. Therefore, PA potentially can provide a reasonable compromise between spatial resolution and imaging depth [77], [78], [83], [131].

Research in PA-based monitoring of brain activity has seen a significant increase in the last couple of years. It was first implemented using calcium-sensitive dyes/probes and GECIs that exhibited a change in the PA signal in response to changes in local calcium flux [14, 19, 20]. However, changes in local calcium concentration are relatively slow and are an indirect measure of brain activity, and do not accurately reflect the changes in cell

membrane potential. More recently, Rao *et al.* reported the first demonstration of PA imaging *in vitro* in HEK-293 cell cultures and *in vivo* on the surface of a mouse brain using a non-radiative voltage sensor named dipicrylamine (DPA) [88]. Despite this success, Rao *et al.* noted that the DPA-based approach was limited to superficial sensing [21] due to the fact that the absorption peak of DPA is centered at 420 nm [22]. Additionally, the optical properties of DPA do not change with changes in cell membrane potential, rather the local concentration of DPA varies due to voltage-dependent translocation of DPA in the lipid bilayer [22]. Therefore, the DPA-based approach requires high-sensitivity in detection of PA signals and are highly dependent on the *in situ* concentration of DPA. The development of voltage-sensitive probes/dyes that are specifically optimized for *in vivo* PA-based sensing remains an active area of research [23, 24].

To facilitate a systematic translation of *in vitro* studies to *in vivo* applications, voltage-reporting probes that can serve both fluorescence and photoacoustic sensing of bioelectric activity are desirable. Ideally, such probes should have the following characteristics: (1) an optical-absorption signature that exhibits a voltage-dependent change in magnitude or spectroscopic shift, (2) temporal response in sub-microsecond scale, and (3) sufficient photostability to enable long-term imaging. Candidate probes for dual-modality voltage-sensing are quantum dots (QDs), which possess the following attributes that make them attractive voltage reporters: (1) quantum-confined stark effect in response to an electric field [25, 26], (2) an ability to engage in electron transfer (ET) processes [27, 28], (3) superior photostability, and (4) an acceptable (low) level of

cytotoxicity [29-31]. Details of this QD-based construct and results from experimental design and characterization are presented below.

4.1. The QD-peptide-C₆₀ construct

The development of a quantum dot (QD)-peptide-fullerene (C₆₀) electron transfer (ET) based nanobioconjugate for the visualization of membrane potential in living cells was recently reported in 2017 by Nag et al. [117]. The nanobioconjugate consists of a (1) central photoexcited QD electron donor, (2) membrane-inserting peptidyl linker and (3) C₆₀ electron acceptor [117], [132]. When introduced to cells, the QD-peptide-C₆₀ construct labels the plasma membrane by inserting the peptide-C₆₀ into the hydrophilic bilayer and the hydrophilic QD remains on the exofacial side of the membrane [117]. Figure 4.1 shows the schematic design of the QD-peptide-C₆₀ bioconjugate with the three peptidyl sequences that they used (JBD1, JBD2, and JBD3), molecular models of QD-peptide-C₆₀ construct, and the construct's response to changes in membrane potential. In this chapter, I will be discussing the feasibility of using these novel QD constructs with PA sensing to detect changes in membrane potential.

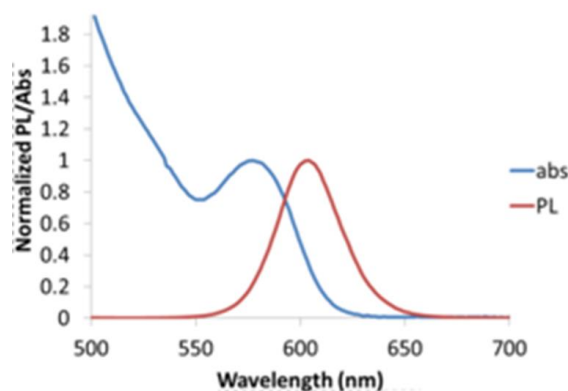


Figure 4.2: Optical-absorption and photoluminescence spectrum of the QD-peptide-C₆₀ bioconjugate. [Courtesy of Dr. James Delehanty-NRL].

4.2. QD-PA sensing of cell depolarization

PC-12 cell cultures were labeled with the voltage-sensing QD-bioconjugate at a concentration of 20 nM (decorated with 20 peptide (JBD1)-C₆₀ per QD). A change in cell membrane potential was chemically induced by increasing the extracellular concentration of KCl. Figure 2.4 in Chapter 2 shows the experimental setup employed for characterizing the PA signal from the QD probes and examining the temporal change in the QD-PA signal during KCl-induced cell depolarization. A 532-nm laser (Phocus Mobile, Opotek, Inc., Carlsbad, CA) with a pulse duration of 5 ns and a pulse-repetition frequency of 10 Hz was used for exciting the QD-probes with an incident fluence of 5 mJ/cm². A focused ultrasound transducer with 20-MHz bandwidth (FWHM beam width of 0.5 mm) detected the PA signals produced by QD-tagged cells in a culture dish. QD-PA signals were amplified using a 20-dB low-noise amplifier (Mini-Circuits, NY, USA) and recorded using a 12-bit digitizer (UHFLI, Zurich Instruments, AG, Switzerland). Figure 4.3 below shows

the PA signal of the QD-labeled cells compared to the tagged cells with peptide-C₆₀ conjugate.

Figure 4.3 shows the photoacoustic response from PC12 cells tagged with the complete QD-based voltage-sensing construct (QD-JBD1peptide-C₆₀) as well as cells tagged with just the peptide-C₆₀ conjugates. As shown, in the absence of the QD, there is negligible PA response, indicating the critical role of the QD in mediating the generation of the PA signal.

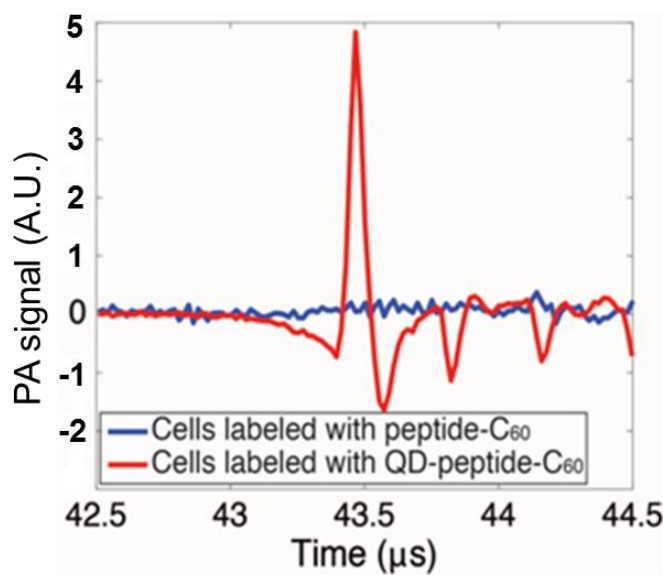


Figure 4.3: PC12 cells tagged with peptide-C₆₀ do not produce an appreciable PA signal. However, cells labeled with QD-peptide-C₆₀ produces a strong PA signal.

The PA signal from the QD-labeled cells was recorded as a function of time with administering four different concentrations of KCl. Figure 4.4 shows the fractional change in PA signal of the labeled cells as a function of time with administering 30 mM KCl in comparison to administering deionized water (0 mM KCl concentration) as a control. The developed theoretical model discussed in Chapter 2 was used to determine the corresponding increase in cell-membrane potential, from the added KCl concentrations of 2.5, 8, 17 and 30 mM, which was determined to be 10, 20, 30, and 40 mV, respectively (see Figure 2.5 in Chapter 2).

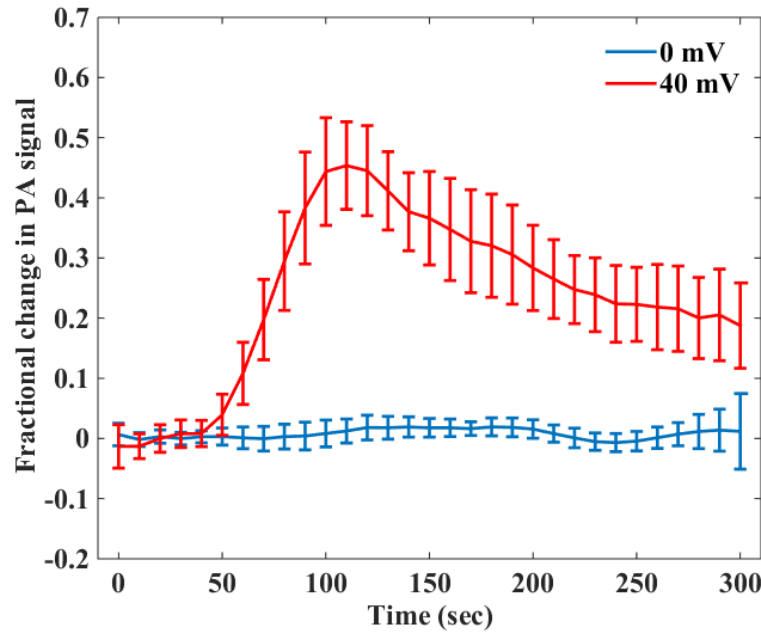


Figure 4.4: Fractional change in PA signal of the QD-labeled cells as a function of time with a 40 mV increase in cell membrane potential. Error bars represent the standard deviation between multiple trials (N=4).

The amplitude of the QD-PA signal was monitored over time while the PC12 cells were depolarized by administering KCl. The QD-PA signals exhibited a dynamic change that was qualitatively and quantitatively similar to the QD-PL results presented by Nag et al. [117]. Both signals exhibited over a 20% change due to KCl-induced depolarization. Furthermore, QD-PA signal tracked the temporal profile of the QD-PL signal in the time course of 150 seconds. Figure 4.5 below shows the fractional change in the PA signal of the QD-labeled cells as a function of change in cell-membrane potential. PA signal demonstrated a monotonic increase with increasing voltage. The dynamics of the change in cell-membrane voltage were consistent with the results of the theoretical model that accounted for KCl diffusion from the edge of the cell-culture dish.

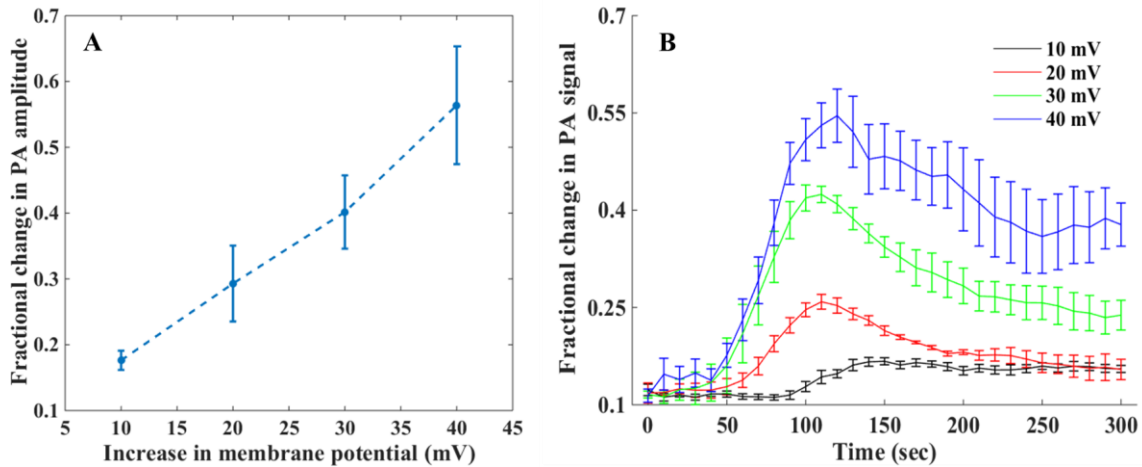


Figure 4.5: (A) Fractional change in the PA amplitude of QD-labeled cells as a function of cell potential. (B) Fractional change in the PA signal of QD-labeled cells as a function of time while changing the membrane potential by administering various KCl

concentrations at 50-second time point. Error bars represent the standard deviation between multiple trials (N=4).

We were curious to know whether or not the extracellular KCl concentrations that we administered had an effect on the cell volume. Therefore, PA measurements of the QD-labeled cells were conducted with administering comparable concentrations of sucrose to those used with KCl (i.e. 2.5 mM as the lowest concentration and 30 mM as the highest concentration used in our experiments). Our findings are presented in Figure 4.6.

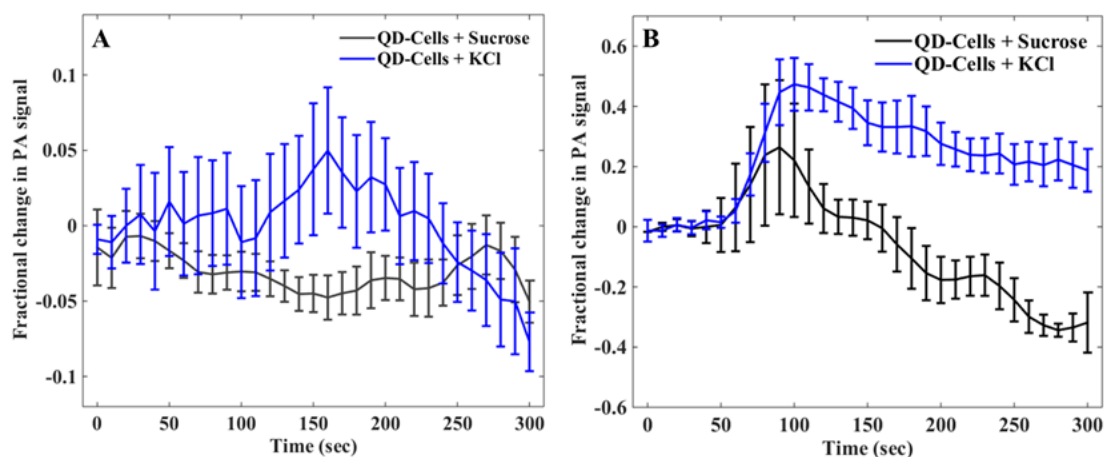


Figure 4.6: Fractional change in PA signal of QD-labeled cells as a function of time while administering KCl and sucrose with the low (A) and relatively high (B) concentrations. Error bars represent the standard deviation between multiple trials (N=3 for the sucrose experiments and N=4 for the KCl experiments).

In addition, PA measurements were performed to determine the optimal concentration of the QD construct that could be used with PC12 cell culture. In our experiments, 20-nM QD concentration was used and we discovered that the optimal concentration to be used is 10-nM and thus it is better to use a lower concentration that could potentially address the cytotoxicity issue. Figure 4.7 shows the fractional change in the QD-PA signal as a function of change in QD concentration while keeping the number of peptide- C_{60} constant (20 JBD1- C_{60} /QD).

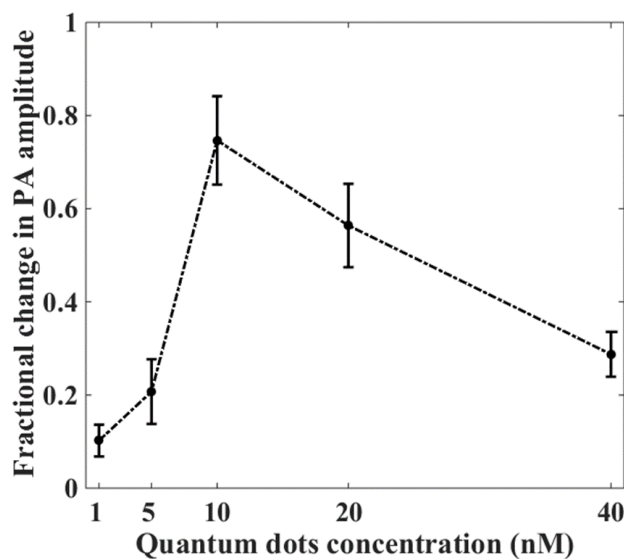


Figure 4.7: Fractional change in QD-PA signal as a function of QD concentration. Error bars represent the standard deviation between multiple trials (N=4).

4.3. Calibration of QD-PL and QD-PA response versus voltage

The QD-PL signal exhibited a fractional change of ~ 0.05 (5%) when the cell membrane potential was increased from resting voltage of -70 mV to 10 mV (see Figure 4.8). Hence, the corresponding QD-PL sensitivity was calculated to be 0.06% per mV, which is comparable to other commercially available voltage-sensitive fluorescence dyes (ANEPPS dyes 0.1% per mV, RH-1691 0.01% per mV [133], [134]). Two-way ANOVA analysis indicated that the mean fractional change in QD-PL for increasing cell membrane potential was statistically different from that at resting potential ($p=0.0003$).

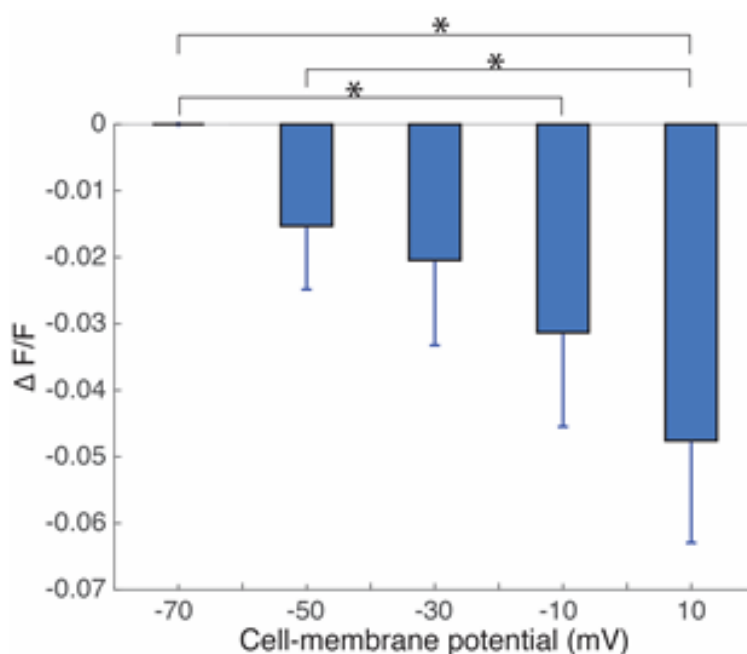


Figure 4.8: Fractional change in QD-PL as a function of cell membrane potential incrementally increased using a whole-cell patch clamp. Bar represents mean QD-PL response and the error bars represent standard error of the means (N=3). * denotes measurements that were statistically different

from each other based on two-way ANOVA analysis [Courtesy of Dr. John R. Cressman and his student intern Ms. Mara Casebeer].

The theoretical model was used as a calibration step and compared with our PA experimental results of the QD-labeled cells as a function of change in membrane potential. The model helps to accurately predict the change in membrane potential based on the added extracellular KCl concentrations. Figure 4.9 shows the fractional change in PA signal response of QD-labeled cells as a function of membrane potential change.

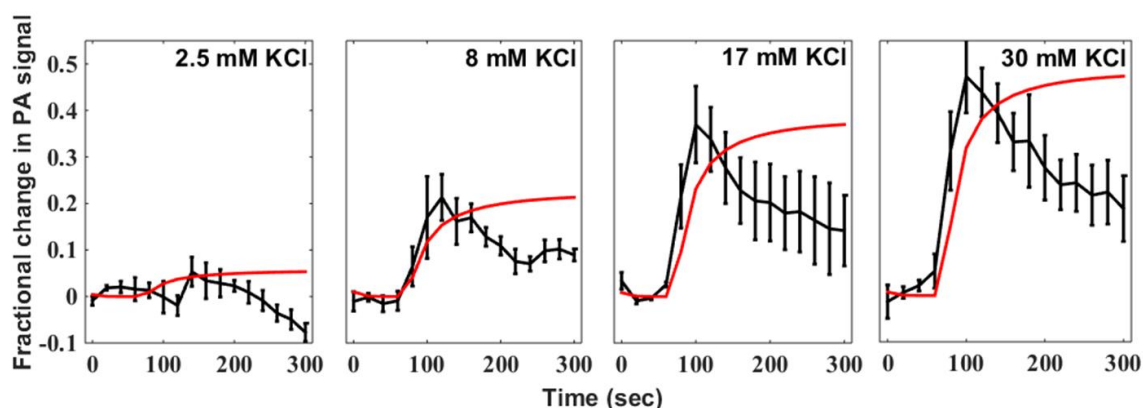


Figure 4.9: Fractional changes in PA-signal amplitude (experimental (in black) versus theoretical model (in red)) of QD-labeled PC12 cells at 532 nm as a function of time as various KCl concentrations were administered (2.5 mM, 8 mM, 17 mM and 30 mM). Error bars represent the standard deviation between multiple trials (N=4).

4.4. Discussion

The feasibility of using a QD-based voltage-sensing construct to remotely detect real-time changes in cellular membrane potential using fluorescence and photoacoustic techniques was demonstrated. The cells were labeled with 20-nM QD-bioconjugate solution. This concentration is 1-2 orders of magnitude smaller than that employed when commercially available VSDs are used to monitor bioelectric activity. Importantly, we observed no deleterious effects on cell viability or activity when interfaced with the QD probe, consistent with our previous studies [32]. Detailed cytotoxicity studies will enable determination of optimal QD probe concentration that can be used for maximizing PL and PA signal-to-noise ratio while ensuring minimal cytotoxic effects.

The current study was limited to demonstrating dual-modality sensing of chemically induced depolarization, which occurs over relatively long time scales (seconds). The QD-PL and QD-PA results were qualitatively and quantitatively consistent with each other. One of the contributing factors to this relatively slow time course is the time necessary for the diffusion of KCl in the cell-culture dish (KCl was administered near the edge of the dish). This limitation was due to the slow pulse-repetition frequency of our excitation laser. QD-PA excitation using a kHz-repetition laser will facilitate QD-PA-based monitoring of real-time spike activity (*e.g.*, action potentials) from electrically active cells.

Our patch-clamp studies offered independent validation of the voltage-sensing response of our QD-probes for comparison against the KCl-induced depolarization, and provide evidence that the change in optical properties of our QD probes is indeed related

to the change in membrane potential. Although the two measurements were qualitatively consistent (in that increase in cell-membrane potential led to an increase in the magnitude of signal change), the QD-PL sensitivity inferred from the patch-clamp experiments was not quantitatively consistent with that from the KCl experiments. One possible reason for this could be the relatively low SNR encountered when using a camera to quantify single-cell QD-PL. This alleviated when using KCl-based depolarization of cell cultures. In these studies, QD-PL sensitivity of our probes was found to be comparable to other commercially available probes such as Fluovolt in head-to-head KCl-depolarization studies [32], the QD-PL sensitivity inferred from the patch-clamp experiments was somewhat below some of the voltage-reporting fluorophores [38]. Because the KCl concentrations employed to depolarize the cells were in the range that are physiological and an order of magnitude lower than those used in recently published works by Rao et al. [21], the change in QD-PL and QD-PA signals is not likely due to KCl-induced osmotic changes in the cell volume. Although this discrepancy warrants furthermore investigation, we conjecture that it could be due to imperfect patching of the relatively small PC12 cells, which might result in a less than prescribe change in the cell-membrane potential.

Although the physical mechanisms involved in the voltage-dependent change in QD-PL signal is relatively well understood [32], the underlying physics involved in voltage-dependent changes in the photoacoustic signal from this QD-peptide-C60 construct is not well elucidated. However, the results presented above indicate that an increase in the PA-signal amplitude is likely associated with ET-enhanced quenching, which can lead to an increase in local heating. Detailed mechanistic studies will facilitate

further optimization of these QD-based probes for dual-modality sensing of bioelectric activity.

In comparison to other photoacoustic voltage-reporting probes demonstrated in recent publications [21, 24], the QD-based probes have the following distinct advantages: 1) high photo-thermal stability [32], 2) comparable sensitivity and behavior for PL and PA sensing (Fig. 4b), 3) PA signal that increases as a function of cell-membrane voltage (alleviating challenges associated with low SNR), and 4) mechanism for changes in signal that do not rely on trans-location of the probe. In comparison to Rao et al. [21], where 5 mM of DPA (voltage reported) was used to achieve a fractional PA-voltage sensitivity of 0.4% per mV, we used 20 nM of QD-probe to achieve a maximum PA-voltage sensitivity of approximately 1% per mV.

Another attractive feature of the QD-bioconjugates is the modular arrangement, which can allow replacing the CdSe QD with another QD that can be excited using near-infrared (NIR) excitation. Such probes will further improve the ability to detect and map bioelectric activity deeper in tissue, which is particularly relevant for studies involving small-animal models.

4.5. Conclusion

In this chapter, we demonstrated that the novel QD-peptide-C₆₀ bioconjugate is a good voltage-sensitive reporter for PAS. The QD construct that was used has a strong emission at 605 nm and 532-nm pulse laser was used in our PAS measurements. We found out that this QD bioconjugate is concentration dependent with the PC12 cell culture studies and that the PA signal increased as an increase in membrane potential. This feature, makes

this construct more attractive reporter than other commercially available VSD such as RH155 that showed decrease in the PA signal as a function of membrane potential and thus the signal dropped to the noise level. Furthermore, this QD bioconjugate is an ideal probe for PA sensing and imaging due to its modular arrangement that allows the replacement of the QD core with another NIR QD.

CHAPTER FIVE: SUMMARY AND FUTURE DIRECTION

In this dissertation, the feasibility of using photoacoustic (PA) sensing of bio-electrical activity using commercially available voltage-sensitive absorption dye RH155 and a novel voltage-sensing 605-nm QD construct has been studied. We have demonstrated sensing of bio-electrical activity using PA-based voltage sensing. We have achieved this in two ways: (1) by characterizing the optical-absorption properties of voltage-sensitive dyes as a function of membrane potential change using a custom absorption spectrophotometer, and (2) by using *in vitro* experiments involving cell cultures to demonstrate that the PA signal from cells labelled with voltage-reporting probes track the change in cell potential. The dynamic characterization of the optical-absorption spectra of various voltage-sensitive dyes/probes, in direct response to membrane potential change, will provide insight into how the optical properties change at time scales that are relevant to real physiological and pathological condition examinations of the various VSDs. Thus, a library of optical-absorption data could be produced and be used to select the optimal voltage-sensing probes for *in vitro* and *in vivo* PA sensing/imaging applications.

We developed *in vitro* protocols to characterize and screen potential voltage-sensitive probes for PA sensing. The PA signature of a commercially available VSD and a novel engineering voltage-sensing QD construct were examined and demonstrated their feasibility for photoacoustically sensing changes in cell-membrane potential. In addition, a computational model to accurately assess the effects on transmembrane potential was established and validated with whole-cell patch clamp.

PA sensing of voltage has the potential to address a significant need of improving sensing depth while providing resolution necessary to investigate signaling in large intact neural circuits. Although turn-key instrumentation for acquiring high-fidelity 2 dimensional and 3 dimensional PA images of rodent brain is commercially available, lack of VSDs optimized for PA sensing is a major hindrance. Potential VSDs should have the following characteristics to be suitable for PA-based imaging of bio- and neuro-electrical activity: (1) optical-absorption peak in the near-infrared to infrared regime for optimal penetration in tissue, (2) optical-absorption signature that exhibits a voltage-dependent change in magnitude or spectroscopic shift, and (3) temporal response in millisecond scale. RH155 dye was chosen because it is an absorption VSD with absorption peak centered at 650 nm and it is commercially available voltage-sensing dye. Because PA signal relies on absorption of light and subsequent thermoelastic expansion of the medium, absorption-based dyes (usually low quantum yield, more heating) will be better suited as PA voltage reporters than conventional fluorescence-based voltage reporters (high quantum yield, less heating). In PA-based approach, the information from VSDs to the sensor is relayed acoustically (instead of optically), therefore, PA-based approach potentially could provide useful sensing and mapping of bioelectric activity deeper in tissue in comparison to the sensing depths possible using fluorescence-based techniques. VSDs that have an absorption peak in the near-infrared regime will further improve sensing depth.

The feasibility of using a QD-based voltage-sensing construct to remotely detect real-time changes in cellular membrane potential using fluorescence and PA techniques was demonstrated. The cells were labeled with 20-nM QD-bioconjugate solution. This

concentration is 1-2 orders of magnitude smaller than that employed when commercially available VSDs are used to monitor bio-electrical activity. Importantly, we observed no deleterious effects on cell viability or activity when interfaced with the QD probe. Detailed cytotoxicity studies using MEAs will enable determination of optimal QD probe concentration that can be used for maximizing PL and PA signal-to-noise ratio while ensuring minimal cytotoxic effects. Although the physical mechanisms involved in the voltage-dependent change in QD-PL signal is relatively well understood [117], the underlying physics involved in voltage-dependent changes in the PA signal from this QD-peptide-C₆₀ bioconjugate is not well elucidated. However, the results presented above indicate that an increase in the PA-signal amplitude is likely associated with electron transfer-enhanced quenching, which can lead to an increase in local heating. Detailed mechanistic studies will facilitate further optimization of these QD-based probes for dual-modality sensing of bio-electrical activity.

The current work was limited to demonstrating QD dual-modality sensing of chemically induced depolarization, which occurs over relatively long time scales (seconds). The current laser was limited to a pulse-repetition frequency of 10 Hz, which does not provide the temporal resolution necessary for resolving neuronal action potentials. KCl-induced “slow” changes in cell-membrane potential provides a convenient model for characterizing the performance of photoacoustic VSDs *in vitro*. *In vivo* implementation of PA-based voltage imaging will require nanosecond-pulsed lasers with a pulse repetition rate 1 kHz or greater [89], [128] in order to resolve action potentials. A kHz-pulsed laser could be utilized along with a low-noise needle hydrophone to excite and visualize the PA

signals from labeled undifferentiated PC12, differentiated PC12, and/or neuronal cell cultures, respectively. In this design, we will be able to simultaneously measure the absorption and the PA signal of the QD-labeled cell culture.

These novel QD-bioconjugates has a modular arrangement that allows the replacement of the current CdSe QD with another QD that can be excited using near-infrared excitation. The response of these NIR voltage-sensing QD probes could be characterized and could demonstrate their PA sensing applications with the current setup that was developed. Furthermore, the feasibility of using NIR voltage-sensitive probes for PA sensing of bio- and neuro-electrical activity *in vitro* and *in vivo* could be demonstrated with the developed PA setup. QD-labeled hippocampal slices could be used to demonstrate the *in vivo* applications of our developed methods. Such voltage-sensing probes will further improve the ability to detect and map bio-electrical activity deeper in tissue, which is particularly relevant for studies involving small-animal models. Another future work could involve the replacement of the single-element ultrasound transducers that were used in this research work with a linear array transducer that will allow simultaneous demonstration of QD-based PA sensing of bioelectrical activity.

Furthermore, with our developed methodologies, we will be able to characterize and test various voltage-sensing probes for optimal PA sensing and imaging applications. For instance, indocyanine green (ICG) – an infrared fluorescent dye with FDA approval as an intravenously administered contrast agent – was reported to be a voltage-sensitive dye [122]. ICG is limited by its concentration-dependent aggregation, rapid degradation, photobleaching, and aqueous instability. One potential approach to overcome these

limitations is to formulate liposome-bound ICG where studies have shown that ICG is completely and stably incorporated into the lipid membrane [135]. Liposome-bound ICG could be used as a contrast agent and voltage-sensitive probe for *in vitro* and *in vivo* PA sensing and imaging.

The key advantage of the PA voltage-based sensing is the ability to image deeper in the brain and noninvasively. PA-based voltage techniques could provide voltage maps with adequate spatiotemporal resolutions and field-of-view for monitoring cell-membrane potential in intact circuits and are potentially better suited for studying brain function in small animal models [77], [131].

REFERENCES

- [1] M. Bébarová, “Advances in patch clamp technique: towards higher quality and quantity,” *Gen. Physiol. Biophys.*, vol. 31, no. 2, pp. 131–140, Jun. 2012.
- [2] L. Oltedal, S. H. Mørkve, M. L. Veruki, and E. Hartveit, “Patch-clamp investigations and compartmental modeling of rod bipolar axon terminals in an in vitro thin-slice preparation of the mammalian retina,” *J. Neurophysiol.*, vol. 97, no. 2, pp. 1171–1187, Feb. 2007.
- [3] D. J. Yao, C. H. Chen, S. H. Tseng, and S. R. Yeh, “Design and Fabrication of Micro Multi-Probe Electrode Arrays,” in *2007 2nd IEEE International Conference on Nano/Micro Engineered and Molecular Systems*, 2007, pp. 96–100.
- [4] L. Berdondini *et al.*, “High-density electrode array for imaging in vitro electrophysiological activity,” *Biosens. Bioelectron.*, vol. 21, no. 1, pp. 167–174, Jul. 2005.
- [5] A. F. M. Johnstone, G. W. Gross, D. G. Weiss, O. H.-U. Schroeder, A. Gramowski, and T. J. Shafer, “Microelectrode arrays: a physiologically based neurotoxicity testing platform for the 21st century,” *Neurotoxicology*, vol. 31, no. 4, pp. 331–350, Aug. 2010.
- [6] H. Charkhkar, G. L. Knaack, B. E. Gnade, E. W. Keefer, and J. J. Pancrazio, “Development and demonstration of a disposable low-cost microelectrode array for cultured neuronal network recording,” *Sens. Actuators B Chem.*, vol. 161, no. 1, pp. 655–660, Jan. 2012.
- [7] L. Griscom, P. Degenaar, B. LePioufle, E. Tamiya, and H. Fujita, “Techniques for patterning and guidance of primary culture neurons on micro-electrode arrays,” *Sens. Actuators B Chem.*, vol. 83, no. 1–3, pp. 15–21, Mar. 2002.
- [8] D. R. Hochbaum *et al.*, “All-optical electrophysiology in mammalian neurons using engineered microbial rhodopsins,” *Nat. Methods*, vol. 11, no. 8, pp. 825–833, Aug. 2014.
- [9] Y. Gong, M. J. Wagner, J. Z. Li, and M. J. Schnitzer, “Imaging neural spiking in brain tissue using FRET-opsin protein voltage sensors,” *Nat. Commun.*, vol. 5, p. 3674, Apr. 2014.
- [10] J. E. González and R. Y. Tsien, “Voltage sensing by fluorescence resonance energy transfer in single cells,” *Biophys. J.*, vol. 69, no. 4, pp. 1272–1280, Oct. 1995.
- [11] D. S. Peterka, H. Takahashi, and R. Yuste, “Imaging voltage in neurons,” *Neuron*, vol. 69, no. 1, pp. 9–21, Jan. 2011.
- [12] D. Wang, Z. Zhang, B. Chanda, and M. B. Jackson, “Improved Probes for Hybrid Voltage Sensor Imaging,” *Biophys. J.*, vol. 99, no. 7, pp. 2355–2365, Oct. 2010.
- [13] R. J. Clarke, A. Zouni, and J. F. Holzwarth, “Voltage sensitivity of the fluorescent probe RH421 in a model membrane system,” *Biophys. J.*, vol. 68, no. 4, pp. 1406–1415, Apr. 1995.
- [14] V. Tsytsarev *et al.*, “Recent progress in voltage-sensitive dye imaging for neuroscience,” *J. Nanosci. Nanotechnol.*, vol. 14, no. 7, pp. 4733–4744, Jul. 2014.

- [15] M. Matson, N. Carlsson, T. Beke-Somfai, and B. Nordén, "Spectral Properties and Orientation of Voltage-Sensitive Dyes in Lipid Membranes," *Langmuir*, vol. 28, no. 29, pp. 10808–10817, Jul. 2012.
- [16] D. Khudhair, S. Nahavandi, H. Garmestani, and A. Bhatti, "Microelectrode Arrays: Architecture, Challenges and Engineering Solutions," in *Emerging Trends in Neuro Engineering and Neural Computation*, Springer, Singapore, 2017, pp. 41–59.
- [17] M. V. Accardi, M. K. Pugsley, R. Forster, E. Troncy, H. Huang, and S. Authier, "The emerging role of in vitro electrophysiological methods in CNS safety pharmacology," *J. Pharmacol. Toxicol. Methods*, vol. 81, pp. 47–59, Sep. 2016.
- [18] A. Stett *et al.*, "Biological application of microelectrode arrays in drug discovery and basic research," *Anal. Bioanal. Chem.*, vol. 377, no. 3, pp. 486–495, Oct. 2003.
- [19] M. D. Johnson, R. K. Franklin, M. D. Gibson, R. B. Brown, and D. R. Kipke, "Implantable microelectrode arrays for simultaneous electrophysiological and neurochemical recordings," *J. Neurosci. Methods*, vol. 174, no. 1, pp. 62–70, Sep. 2008.
- [20] M. W. Merlo, R. L. Snyder, J. C. Middlebrooks, and M. Bachman, "Microelectrode arrays fabricated using a novel hybrid microfabrication method," *Biomed. Microdevices*, vol. 14, no. 1, pp. 193–205, Feb. 2012.
- [21] J. P. Seymour, N. B. Langhals, D. J. Anderson, and D. R. Kipke, "Novel multi-sided, microelectrode arrays for implantable neural applications," *Biomed. Microdevices*, vol. 13, no. 3, pp. 441–451, Jun. 2011.
- [22] H. Charkhkar, G. L. Knaack, H. S. Mandal, E. W. Keefer, and J. J. Pancrazio, "Effects of carbon nanotube and conducting polymer coated microelectrodes on single-unit recordings in vitro," *Conf. Proc. Annu. Int. Conf. IEEE Eng. Med. Biol. Soc. IEEE Eng. Med. Biol. Soc. Annu. Conf.*, vol. 2014, pp. 469–473, 2014.
- [23] T. Ryyänen *et al.*, "All Titanium Microelectrode Array for Field Potential Measurements from Neurons and Cardiomyocytes: A Feasibility Study," 2011.
- [24] M. E. J. Obien, K. Deligkaris, T. Bullmann, D. J. Bakkum, and U. Frey, "Revealing neuronal function through microelectrode array recordings," *Front. Neurosci.*, vol. 8, Jan. 2015.
- [25] "Patch clamp techniques for single channel and whole-cell recording," *Science Mission*. <http://sciencemission.com/site/index.php?page=news&type=view&id=protocols%2Fpatch-clamp-techniques>.
- [26] M. Karmazínová and L. Lacinová, "Measurement of cellular excitability by whole cell patch clamp technique," *Physiol. Res.*, vol. 59 Suppl 1, pp. S1-7, 2010.
- [27] R. X. Faria, L. G. B. Ferreira, and L. A. Alves, "The Mystery of P2X7 Ionotropic Receptor: From a Small Conductance Channel to a Large Conductance Channel," *Neurosci. - Deal. Front.*, 2012.
- [28] D. Khodagholy *et al.*, "In vivo recordings of brain activity using organic transistors," *Nat. Commun.*, pp. 4, 1575, 2013.
- [29] M. A. Nicolelis, *Methods for Neural Ensemble Recordings*. CRC Press/Taylor & Francis, 2008.

- [30] R. C. Roberts and N. C. Tien, "3D printed stainless steel microelectrode arrays," in *2017 19th International Conference on Solid-State Sensors, Actuators and Microsystems (TRANSDUCERS)*, 2017, pp. 1233–1236.
- [31] P. J. Rousche and R. A. Normann, "Chronic recording capability of the Utah Intracortical Electrode Array in cat sensory cortex," *J. Neurosci. Methods*, vol. 82, no. 1, pp. 1–15, Jul. 1998.
- [32] T. Stieglitz, P. Heiduschka, M. Schuettler, and M. Gross, "Reducing insertion sites of penetrating multipolar shaft electrodes by double side electrode arrangement," in *2001 Conference Proceedings of the 23rd Annual International Conference of the IEEE Engineering in Medicine and Biology Society*, 2001, vol. 4, pp. 3426–3429 vol.4.
- [33] T. J. Blanche, M. A. Spacek, J. F. Hetke, and N. V. Swindale, "Polytrodes: high-density silicon electrode arrays for large-scale multiunit recording," *J. Neurophysiol.*, vol. 93, no. 5, pp. 2987–3000, May 2005.
- [34] U. Frey *et al.*, "126 channel-CMOS microelectrode array for electrogenic cells," in *2007 IEEE 20th International Conference on Micro Electro Mechanical Systems (MEMS)*, 2007, pp. 541–544.
- [35] A. Blau *et al.*, "Flexible, all-polymer microelectrode arrays for the capture of cardiac and neuronal signals," *Biomaterials*, vol. 32, no. 7, pp. 1778–1786, Mar. 2011.
- [36] G. Buzsáki, "Large-scale recording of neuronal ensembles," *Nat. Neurosci.*, vol. 7, no. 5, pp. 446–451, May 2004.
- [37] S. Musallam, M. J. Bak, P. R. Troyk, and R. A. Andersen, "A floating metal microelectrode array for chronic implantation," *J. Neurosci. Methods*, vol. 160, no. 1, pp. 122–127, Feb. 2007.
- [38] T. Kim, P. R. Troyk, and M. Bak, "Active floating micro electrode arrays (AFMA)," *Conf. Proc. Annu. Int. Conf. IEEE Eng. Med. Biol. Soc. IEEE Eng. Med. Biol. Soc. Annu. Conf.*, vol. 1, pp. 2807–2810, 2006.
- [39] M. Shtrahman, D. B. Aharoni, N. F. Hardy, D. V. Buonomano, K. Arisaka, and T. S. Otis, "Multifocal fluorescence microscope for fast optical recordings of neuronal action potentials," *Biophys. J.*, vol. 108, no. 3, pp. 520–529, Feb. 2015.
- [40] P. P. Mondal and A. Diaspro, *Fundamentals of Fluorescence Microscopy: Exploring Life with Light*. Springer Netherlands, 2014.
- [41] A. Miyawaki, "Innovations in the imaging of brain functions using fluorescent proteins," *Neuron*, vol. 48, no. 2, pp. 189–199, Oct. 2005.
- [42] K. L. Rogers *et al.*, "Non-Invasive In Vivo Imaging of Calcium Signaling in Mice," *PLOS ONE*, vol. 2, no. 10, p. e974, Oct. 2007.
- [43] R. Y. Tsien, T. Pozzan, and T. J. Rink, "T-cell mitogens cause early changes in cytoplasmic free Ca^{2+} and membrane potential in lymphocytes," *Nature*, vol. 295, no. 5844, pp. 68–71, Jan. 1982.
- [44] M. D. Bootman, K. Rietdorf, T. Collins, S. Walker, and M. Sanderson, " Ca^{2+} -sensitive fluorescent dyes and intracellular Ca^{2+} imaging," *Cold Spring Harb. Protoc.*, vol. 2013, no. 2, pp. 83–99, Feb. 2013.
- [45] H. Ma *et al.*, "Wide-field in vivo neocortical calcium dye imaging using a convection-enhanced loading technique combined with simultaneous

- multiwavelength imaging of voltage-sensitive dyes and hemodynamic signals,” *Neurophotronics*, vol. 1, no. 1, Jul. 2014.
- [46] V. Pérez Koldenkova and T. Nagai, “Genetically encoded Ca^{2+} indicators: Properties and evaluation,” *Biochim. Biophys. Acta BBA - Mol. Cell Res.*, vol. 1833, no. 7, pp. 1787–1797, Jul. 2013.
 - [47] L. Tian, S. A. Hires, and L. L. Looger, “Imaging Neuronal Activity with Genetically Encoded Calcium Indicators,” *Cold Spring Harb. Protoc.*, vol. 2012, no. 6, p. pdb.top069609, Jun. 2012.
 - [48] M. Cameron *et al.*, “Calcium Imaging of AM Dyes Following Prolonged Incubation in Acute Neuronal Tissue,” *PLOS ONE*, vol. 11, no. 5, p. e0155468, May 2016.
 - [49] S. H.-E.-R. Mullah *et al.*, “Evaluation of voltage-sensitive fluorescence dyes for monitoring neuronal activity in the embryonic central nervous system,” *J. Membr. Biol.*, vol. 246, no. 9, pp. 679–688, Sep. 2013.
 - [50] N. Vogt, “Voltage sensors: challenging, but with potential,” *Nat. Methods*, vol. 12, no. 10, pp. 921–924, Oct. 2015.
 - [51] B. P. Bammel *et al.*, “NMR, calorimetric, spin-label, and optical studies on a trifluoromethyl-substituted styryl molecular probe in dimyristoylphosphatidylcholine vesicles and multilamellar suspensions: a model for location of optical probes,” *Biochim. Biophys. Acta*, vol. 1024, no. 1, pp. 61–81, May 1990.
 - [52] L. M. Loew, G. W. Bonneville, and J. Surow, “Charge shift optical probes of membrane potential. Theory,” *Biochemistry (Mosc.)*, vol. 17, no. 19, pp. 4065–4071, Sep. 1978.
 - [53] A. S. Waggoner and A. Grinvald, “Mechanisms of rapid optical changes of potential sensitive dyes,” *Ann. N. Y. Acad. Sci.*, vol. 303, pp. 217–241, Dec. 1977.
 - [54] W. Liptay, “Electrochromism and Solvatochromism,” *Angew. Chem. Int. Ed. Engl.*, vol. 8, no. 3, pp. 177–188, Mar. 1969.
 - [55] Y. Momose-Sato, K. Sato, Y. Arai, I. Yazawa, H. Mochida, and K. Kamino, “Evaluation of voltage-sensitive dyes for long-term recording of neural activity in the hippocampus,” *J. Membr. Biol.*, vol. 172, no. 2, pp. 145–157, Nov. 1999.
 - [56] F. Zhang *et al.*, “Optogenetic interrogation of neural circuits: technology for probing mammalian brain structures,” *Nat. Protoc.*, vol. 5, no. 3, pp. 439–456, Mar. 2010.
 - [57] S. Yagodin, C. Collin, D. L. Alkon, N. F. Sheppard, and D. B. Sattelle, “Mapping membrane potential transients in crayfish (*Procambarus clarkii*) optic lobe neuropils with voltage-sensitive dyes,” *J. Neurophysiol.*, vol. 81, no. 1, pp. 334–344, Jan. 1999.
 - [58] W. N. Frost *et al.*, “Monitoring Spiking Activity of Many Individual Neurons in Invertebrate Ganglia,” *Adv. Exp. Med. Biol.*, vol. 859, pp. 127–145, 2015.
 - [59] T. D. Parsons, B. M. Salzberg, A. L. Obaid, F. Raccuia-Behling, and D. Kleinfeld, “Long-term optical recording of patterns of electrical activity in ensembles of cultured *Aplysia* neurons,” *J. Neurophysiol.*, vol. 66, no. 1, pp. 316–333, Jul. 1991.
 - [60] W. N. Frost, J. Wang, and C. J. Brandon, “A stereo-compound hybrid microscope for combined intracellular and optical recording of invertebrate neural network activity,” *J. Neurosci. Methods*, vol. 162, no. 1–2, pp. 148–154, May 2007.

- [61] W. Akemann, H. Mutoh, A. Perron, J. Rossier, and T. Knöpfel, “Imaging brain electric signals with genetically targeted voltage-sensitive fluorescent proteins,” *Nat. Methods*, vol. 7, no. 8, pp. 643–649, Aug. 2010.
- [62] T. Knöpfel, J. Díez-García, and W. Akemann, “Optical probing of neuronal circuit dynamics: genetically encoded versus classical fluorescent sensors,” *Trends Neurosci.*, vol. 29, no. 3, pp. 160–166, Mar. 2006.
- [63] K. M. Tyner, R. Kopelman, and M. A. Philbert, “‘Nanosized Voltmeter’ Enables Cellular-Wide Electric Field Mapping,” *Biophys. J.*, vol. 93, no. 4, pp. 1163–1174, Aug. 2007.
- [64] S. M. Buck, H. Xu, M. Brasuel, M. A. Philbert, and R. Kopelman, “Nanoscale probes encapsulated by biologically localized embedding (PEBBLEs) for ion sensing and imaging in live cells,” *Talanta*, vol. 63, no. 1, pp. 41–59, May 2004.
- [65] S. C. Warren, D. A. Walker, and B. A. Grzybowski, “Plasmoelectronics: Coupling Plasmonic Excitation with Electron Flow,” *Langmuir*, vol. 28, no. 24, pp. 9093–9102, Jun. 2012.
- [66] J. Zhang, T. Atay, and A. V. Nurmikko, “Optical detection of brain cell activity using plasmonic gold nanoparticles,” *Nano Lett.*, vol. 9, no. 2, pp. 519–524, Feb. 2009.
- [67] B. K. Juluri, Y. B. Zheng, D. Ahmed, L. Jensen, and T. J. Huang, “Effects of Geometry and Composition on Charge-Induced Plasmonic Shifts in Gold Nanoparticles,” *J. Phys. Chem. C*, vol. 112, no. 19, pp. 7309–7317, May 2008.
- [68] I. Choi and Y. Choi, “Plasmonic Nanosensors: Review and Prospect,” *IEEE J. Sel. Top. Quantum Electron.*, vol. 18, no. 3, pp. 1110–1121, May 2012.
- [69] G. Garcia *et al.*, “Dynamically Modulating the Surface Plasmon Resonance of Doped Semiconductor Nanocrystals,” *Nano Lett.*, vol. 11, no. 10, pp. 4415–4420, Oct. 2011.
- [70] J. D. Marshall and M. J. Schnitzer, “Optical Strategies for Sensing Neuronal Voltage Using Quantum Dots and Other Semiconductor Nanocrystals,” *ACS Nano*, vol. 7, no. 5, pp. 4601–4609, May 2013.
- [71] D. E. M. Invit Joseph A. Bartel, Dr Weiwen Zhao, Dr Imad Naasani, Dr Michael J. Ignatius, Dr Joseph A. Treadway, Dr Alex Savtchenko, “Quantum Dots Move Beyond Fluorescence Imaging.” <https://www.photonics.com/a33995>.
- [72] I. L. Medintz, H. T. Uyeda, E. R. Goldman, and H. Mattoussi, “Quantum dot bioconjugates for imaging, labelling and sensing,” *Nat. Mater.*, vol. 4, no. 6, pp. 435–446, Jun. 2005.
- [73] G. Bardi *et al.*, “The biocompatibility of amino functionalized CdSe/ZnS quantum-dot-Doped SiO₂ nanoparticles with primary neural cells and their gene carrying performance,” *Biomaterials*, vol. 31, no. 25, pp. 6555–6566, Sep. 2010.
- [74] M. A. Ansari and E. Mohajerani, “Mechanisms of Laser-Tissue Interaction: Optical Properties of Tissue,” *J. Lasers Med. Sci.*, vol. 2, no. 3, pp. 119–125, 2011.
- [75] M. H. Niemz, *Laser-Tissue Interactions: Fundamentals and Applications*. Springer Science & Business Media, 2013.

- [76] H. Kobayashi, M. Ogawa, R. Alford, P. L. Choyke, and Y. Urano, "New Strategies for Fluorescent Probe Design in Medical Diagnostic Imaging," *Chem. Rev.*, vol. 110, no. 5, pp. 2620–2640, May 2010.
- [77] J. Yao and L. V. Wang, "Photoacoustic brain imaging: from microscopic to macroscopic scales," *Neurophotonics*, vol. 1, no. 1, pp. 011003–011003, 2014.
- [78] D. Wang, Y. Wu, and J. Xia, "Review on photoacoustic imaging of the brain using nanoprobes," *Neurophotonics*, vol. 3, no. 1, p. 010901, Jan. 2016.
- [79] N. Dana, R. A. Fowler, A. Allen, J. Zoldan, L. Suggs, and S. Emelianov, "In vitro photoacoustic sensing of calcium dynamics with arsenazo III," *Laser Phys. Lett.*, vol. 13, no. 7, p. 075603, 2016.
- [80] L. V. Wang and S. Hu, "Photoacoustic tomography: in vivo imaging from organelles to organs," *Science*, vol. 335, no. 6075, pp. 1458–1462, Mar. 2012.
- [81] J. Yao and L. V. Wang, "Photoacoustic microscopy," *Laser Photonics Rev.*, vol. 7, no. 5, pp. 758–778, Sep. 2013.
- [82] E. Bossy and S. Gigan, "Photoacoustics with coherent light," *Photoacoustics*, vol. 4, no. 1, pp. 22–35, Mar. 2016.
- [83] S. Hu and L. V. Wang, "Neurovascular Photoacoustic Tomography," *Front. Neuroenergetics*, vol. 2, Jun. 2010.
- [84] X. Wang, G. Ku, M. A. Wegiel, D. J. Bornhop, G. Stoica, and L. V. Wang, "Noninvasive photoacoustic angiography of animal brains in vivo with near-infrared light and an optical contrast agent," *Opt. Lett.*, vol. 29, no. 7, pp. 730–732, Apr. 2004.
- [85] D. Razansky *et al.*, "Multispectral opto-acoustic tomography of deep-seated fluorescent proteins *in vivo*," *Nat. Photonics*, vol. 3, no. 7, pp. 412–417, Jul. 2009.
- [86] G. S. Filonov, A. Krumholz, J. Xia, J. Yao, L. V. Wang, and V. V. Verkhusha, "Deep-Tissue Photoacoustic Tomography of a Genetically Encoded Near-Infrared Fluorescent Probe," *Angew. Chem. Int. Ed.*, vol. 51, no. 6, pp. 1448–1451, Feb. 2012.
- [87] H. Xu *et al.*, "Nanoscale optical probes for cellular imaging," *Chem. Soc. Rev.*, vol. 43, no. 8, pp. 2650–2661, Mar. 2014.
- [88] B. Rao, R. Zhang, L. Li, J.-Y. Shao, and L. V. Wang, "Photoacoustic imaging of voltage responses beyond the optical diffusion limit," *Sci. Rep.*, vol. 7, May 2017.
- [89] E. W. Stein, K. Maslov, and L. V. Wang, "Noninvasive, in vivo imaging of blood-oxygenation dynamics within the mouse brain using photoacoustic microscopy," *J. Biomed. Opt.*, vol. 14, no. 2, p. 020502, Apr. 2009.
- [90] E. W. Stein, K. Maslov, and L. V. Wang, "Noninvasive, in vivo imaging of the mouse brain using photoacoustic microscopy," *J. Appl. Phys.*, vol. 105, no. 10, p. 102027, May 2009.
- [91] H. F. Zhang, K. Maslov, M. Sivaramakrishnan, G. Stoica, and L. V. Wang, "Imaging of hemoglobin oxygen saturation variations in single vessels in vivo using photoacoustic microscopy," *Appl. Phys. Lett.*, vol. 90, no. 5, p. 053901, Jan. 2007.
- [92] X. Wang, Y. Pang, G. Ku, G. Stoica, and L. V. Wang, "Three-dimensional laser-induced photoacoustic tomography of mouse brain with the skin and skull intact," *Opt. Lett.*, vol. 28, no. 19, pp. 1739–1741, Oct. 2003.

- [93] J. Laufer, E. Zhang, G. Raivich, and P. Beard, "Three-dimensional noninvasive imaging of the vasculature in the mouse brain using a high resolution photoacoustic scanner," *Appl. Opt.*, vol. 48, no. 10, pp. D299-306, Apr. 2009.
- [94] L. Xiang, B. Wang, L. Ji, and H. Jiang, "4-D Photoacoustic Tomography," *Sci. Rep.*, vol. 3, p. 1113, Jan. 2013.
- [95] Q. Fan *et al.*, "Perylene-Diimide-Based Nanoparticles as Highly Efficient Photoacoustic Agents for Deep Brain Tumor Imaging in Living Mice," *Adv. Mater.*, vol. 27, no. 5, pp. 843–847, Feb. 2015.
- [96] Z. Guo, S. Hu, and L. V. Wang, "Calibration-free absolute quantification of optical absorption coefficients using acoustic spectra in three-dimensional photoacoustic microscopy of biological tissue," *Opt. Lett.*, vol. 35, no. 12, pp. 2067–2069, 2010.
- [97] A. Mishra, Y. Jiang, S. Roberts, V. Ntziachristos, and G. G. Westmeyer, "Near-Infrared Photoacoustic Imaging Probe Responsive to Calcium," *Anal. Chem.*, vol. 88, no. 22, pp. 10785–10789, Nov. 2016.
- [98] X. L. Deán-Ben *et al.*, "Functional optoacoustic neuro-tomography for scalable whole-brain monitoring of calcium indicators," *Light Sci. Appl.*, vol. 5, no. 12, p. e16201, Dec. 2016.
- [99] H. K. Zhang *et al.*, "Listening to membrane potential: photoacoustic voltage-sensitive dye recording," *J. Biomed. Opt.*, vol. 22, no. 4, p. 045006, Apr. 2017.
- [100] D. S. Peterka, H. Takahashi, and R. Yuste, "Imaging voltage in neurons," *Neuron*, vol. 69, no. 1, pp. 9–21, Jan. 2011.
- [101] C. Liu *et al.*, "Advances in Imaging Techniques and Genetically Encoded Probes for Photoacoustic Imaging," *Theranostics*, vol. 6, no. 13, pp. 2414–2430, Oct. 2016.
- [102] L. A. Greene and A. S. Tischler, "Establishment of a noradrenergic clonal line of rat adrenal pheochromocytoma cells which respond to nerve growth factor," *Proc. Natl. Acad. Sci. U. S. A.*, vol. 73, no. 7, pp. 2424–2428, Jul. 1976.
- [103] A. Orłowska *et al.*, "The Effect of Coatings and Nerve Growth Factor on Attachment and Differentiation of Pheochromocytoma Cells," *Mater. Basel Switz.*, vol. 11, no. 1, Dec. 2017.
- [104] M. J. Eaton and H. Duplan, "Useful cell lines derived from the adrenal medulla," *Mol. Cell. Endocrinol.*, vol. 228, no. 1–2, pp. 39–52, Dec. 2004.
- [105] R. H. S. Westerink and A. G. Ewing, "The PC12 cell as model for neurosecretion," *Acta Physiol. Oxf. Engl.*, vol. 192, no. 2, pp. 273–285, Feb. 2008.
- [106] T. L. Colliver, E. J. Hess, E. N. Pothos, D. Sulzer, and A. G. Ewing, "Quantitative and statistical analysis of the shape of amperometric spikes recorded from two populations of cells," *J. Neurochem.*, vol. 74, no. 3, pp. 1086–1097, Mar. 2000.
- [107] C. M. Grau and L. A. Greene, "Use of PC12 Cells and Rat Superior Cervical Ganglion Sympathetic Neurons as Models for Neuroprotective Assays Relevant to Parkinson's Disease," *Methods Mol. Biol. Clifton NJ*, vol. 846, pp. 201–211, 2012.
- [108] L. A. Greene, "Nerve growth factor prevents the death and stimulates the neuronal differentiation of clonal PC12 pheochromocytoma cells in serum-free medium," *J. Cell Biol.*, vol. 78, no. 3, pp. 747–755, Sep. 1978.

- [109] L. A. Greene and G. Rein, "Release of (3H)norepinephrine from a clonal line of pheochromocytoma cells (PC12) by nicotinic cholinergic stimulation," *Brain Res.*, vol. 138, no. 3, pp. 521–528, Dec. 1977.
- [110] T. L. Colliver, E. J. Hess, E. N. Pothos, D. Sulzer, and A. G. Ewing, "Quantitative and statistical analysis of the shape of amperometric spikes recorded from two populations of cells," *J. Neurochem.*, vol. 74, no. 3, pp. 1086–1097, Mar. 2000.
- [111] R. H. S. Westerink and A. G. Ewing, "The PC12 cell as model for neurosecretion," *Acta Physiol. Oxf. Engl.*, vol. 192, no. 2, pp. 273–285, Feb. 2008.
- [112] P. W. Mesner, T. R. Winters, and S. H. Green, "Nerve growth factor withdrawal-induced cell death in neuronal PC12 cells resembles that in sympathetic neurons," *J. Cell Biol.*, vol. 119, no. 6, pp. 1669–1680, Dec. 1992.
- [113] C. E. Schmidt, V. R. Shastri, J. P. Vacanti, and R. Langer, "Stimulation of neurite outgrowth using an electrically conducting polymer," *Proc. Natl. Acad. Sci. U. S. A.*, vol. 94, no. 17, pp. 8948–8953, Aug. 1997.
- [114] H. K. Kleinman, L. Luckenbill-Edds, F. W. Cannon, and G. C. Sephel, "Use of extracellular matrix components for cell culture," *Anal. Biochem.*, vol. 166, no. 1, pp. 1–13, Oct. 1987.
- [115] A. R. Vancha, S. Govindaraju, K. V. Parsa, M. Jasti, M. González-García, and R. P. Ballester, "Use of polyethyleneimine polymer in cell culture as attachment factor and lipofection enhancer," *BMC Biotechnol.*, vol. 4, p. 23, Oct. 2004.
- [116] J. R. King and N. Kabbani, "Alpha 7 nicotinic receptor coupling to heterotrimeric G proteins modulates RhoA activation, cytoskeletal motility, and structural growth," *J. Neurochem.*, vol. 138, no. 4, pp. 532–545, Aug. 2016.
- [117] O. K. Nag *et al.*, "Quantum Dot–Peptide–Fullerene Bioconjugates for Visualization of in Vitro and in Vivo Cellular Membrane Potential," *ACS Nano*, vol. 11, no. 6, pp. 5598–5613, Jun. 2017.
- [118] J. F. Holtzwarth, V. Eck, and A. Genz, "Iodine laser temperature jump from picosecond to seconds: relaxation processes of phospholipid bilayers," *Spectrosc. Dyn. Biol. Syst. PM Bayley R Dale Ed. Acad. Press Lond.*, pp. 351–377, 1984.
- [119] S. Preuss and W. Stein, "Comparison of Two Voltage-Sensitive Dyes and Their Suitability for Long-Term Imaging of Neuronal Activity," *PLOS ONE*, vol. 8, no. 10, p. e75678, Oct. 2013.
- [120] W. Jin, R.-J. Zhang, and J. Wu, "Voltage-sensitive dye imaging of population neuronal activity in cortical tissue," *J. Neurosci. Methods*, vol. 115, no. 1, pp. 13–27, Mar. 2002.
- [121] D. Zecevic *et al.*, "Imaging Nervous System Activity with Voltage-Sensitive Dyes," *Curr. Protoc. Neurosci.*, vol. 23, no. 1, pp. 6.17.1–6.17.29, Apr. 2003.
- [122] J. S. Treger, M. F. Priest, R. Iezzi, and F. Bezanilla, "Real-time imaging of electrical signals with an infrared FDA-approved dye," *Biophys. J.*, vol. 107, no. 6, pp. L09–12, Sep. 2014.
- [123] J. R. Cressman, G. Ullah, J. Ziburkus, S. J. Schiff, and E. Barreto, "The influence of sodium and potassium dynamics on excitability, seizures, and the stability of persistent states: I. Single neuron dynamics," *J. Comput. Neurosci.*, vol. 26, no. 2, pp. 159–170, Apr. 2009.

- [124] J. A. Payne, C. Rivera, J. Voipio, and K. Kaila, "Cation-chloride co-transporters in neuronal communication, development and trauma," *Trends Neurosci.*, vol. 26, no. 4, pp. 199–206, Apr. 2003.
- [125] O. P. Hamill, A. Marty, E. Neher, B. Sakmann, and F. J. Sigworth, "Improved patch-clamp techniques for high-resolution current recording from cells and cell-free membrane patches," *Pflugers Arch.*, vol. 391, no. 2, pp. 85–100, Aug. 1981.
- [126] W. H. Zhu, L. Conforti, M. F. Czyzyk-Krzeska, and D. E. Millhorn, "Membrane depolarization in PC-12 cells during hypoxia is regulated by an O₂-sensitive K⁺ current," *Am. J. Physiol.*, vol. 271, no. 2 Pt 1, pp. C658–665, Aug. 1996.
- [127] C. Cheung, J. Lee, J. Lee, and O. Shevchuk, "The Effect of Ionic (NaCl) and Non-ionic (Sucrose) Osmotic Stress on the Expression of β -galactosidase in Wild Type E.coli BW25993 and in the Isogenic BW25993 Δ lacI Mutant," *JEMI*, vol. 13, pp. 1–6, Apr. 2009.
- [128] L. V. Wang and J. Yao, "A Practical Guide to Photoacoustic Tomography in the Life Sciences," *Nat. Methods*, vol. 13, no. 8, pp. 627–638, Jul. 2016.
- [129] S. Chemla and F. Chavane, "Voltage-sensitive dye imaging: Technique review and models," *J. Physiol. Paris*, vol. 104, no. 1–2, pp. 40–50, Mar. 2010.
- [130] A. Grinvald and R. Hildesheim, "VSFI: a new era in functional imaging of cortical dynamics," *Nat. Rev. Neurosci.*, vol. 5, no. 11, pp. 874–885, Nov. 2004.
- [131] J. Yao *et al.*, "High-speed label-free functional photoacoustic microscopy of mouse brain in action," *Nat. Methods*, vol. 12, no. 5, pp. 407–410, May 2015.
- [132] M. H. Stewart *et al.*, "Competition between Förster Resonance Energy Transfer and Electron Transfer in Stoichiometrically Assembled Semiconductor Quantum Dot–Fullerene Conjugates," *ACS Nano*, vol. 7, no. 10, pp. 9489–9505, Oct. 2013.
- [133] L. M. Loew *et al.*, "A naphthyl analog of the aminostyryl pyridinium class of potentiometric membrane dyes shows consistent sensitivity in a variety of tissue, cell, and model membrane preparations," *J. Membr. Biol.*, vol. 130, no. 1, pp. 1–10, Oct. 1992.
- [134] V. Tsytsarev, K. Premachandra, D. Takeshita, and S. Bahar, "Imaging cortical electrical stimulation in vivo: fast intrinsic optical signal versus voltage-sensitive dyes," *Opt. Lett.*, vol. 33, no. 9, pp. 1032–1034, May 2008.
- [135] J. C. Kraft and R. J. Y. Ho, "Interactions of indocyanine green and lipid in enhancing near-infrared fluorescence properties: the basis for near-infrared imaging in vivo," *Biochemistry (Mosc.)*, vol. 53, no. 8, pp. 1275–1283, Mar. 2014.

BIOGRAPHY

Nashaat S. Rasheed received his Bachelor of Science degree in Computer and Communication Engineering with two minors in Biomedical Engineering and Biomedical Sciences from the American University of Science and Technology (AUST, Beirut, Lebanon) in 2007. He received his first Master of Engineering degree in Biomedical Engineering from Huazhong University of Science and Technology (HUST, Wuhan, Hubei, China) in 2012, and his second Master of Engineering degree in Biomedical Engineering, from Cornell University (Ithaca, NY, USA) in 2014. He started his PhD program at George Mason University in August of 2014.